Radio-Over-Fiber Dual-Parallel Mach-Zehnder Modulator System for Photonic Generation of Millimeter-Wave Signals Through Two Stages

Fabio Barros de Sousa (fabiufpa@gmail.com)
Universidade Federal do Para https://orcid.org/0000-0003-4170-5261
Fiterlinge M. de Sousa
Universidade Federal do Para
Igor R. S. Miranda
Universidade Federal do Para
Waldomiro Paschoal Jr
Universidade Federal do Pará
Marcos B. C. Costa
Universidade Federal do Para

Research Article

Keywords: Radio-over-Fiber, Dual-Parallel Mach-Zehnder Modulator, NRZ, RZ, Gaussian

Posted Date: March 15th, 2021

DOI: https://doi.org/10.21203/rs.3.rs-285332/v1

Radio-over-Fiber Dual-Parallel Mach-Zehnder Modulator System for Photonic Generation of Millimeter-Wave Signals Through Two Stages

Fabio B. de Sousa[*1,4], Fiterlinge M. de Sousa[1,4], Igor R. S. Miranda[1,4], Waldomiro Paschoal Jr.[*2,4] and Marcos B. C. Costa[1,3,4]

*fabiufpa@gmail.com, *wpaschoaljr@ufpa.br

[1]Universidade Federal do Pará, Programa de Pós-Graduação em Engenharia Elétrica, Rua Augusto Corrêa, 01, Belém, Pará, 66.075-110, Brasil.
[2]Universidade Federal do Pará, Programa de Pós-Graduação em Física, Rua Augusto Corrêa, 01, Belém, Pará, 66.075-110, Brasil.
[3]Universidade Federal do Pará, Faculdade de Engenharia de Materiais, Rodovia BR-316, km 7, Levilândia, Ananindeua, Pará, 67.000-000, Brasil.
[4]Grupo de Pesquisa em Fotônica e Óptica não-Linear. http://dgp.cnpq.br/dgp/espelhogrupo/8017792785061258

ABSTRACT

In this work, we presented a radio-over-fiber (ROF) access network through two modulation stages for the generation of multiple millimeter wave (mm-wave) signals with frequencies of 20GHz, 40GHz, 60GHz and 80 GHz for the transmission rate of 10 Gbps as a function of the variation of link distance and signal power. The specific purpose of the paper was to design and to investigate a RoF system based on the variation of mm-wave frequencies in order to implement a simple and effective system. In stage 1, there are two modulators in parallel (MZM_a and MZM_b) called dual-parallel Mach-Zehnder modulator (DP-MZM) and in stage 2 there is only one modulator (MZM_c), connected to three pulse generators: Non-Return-to-Zero (NRZ), Return-to-Zero (RZ). A single-mode fiber (SMF) and Gaussian and an erbium-doped fiber amplifier (EDFA) were also used to send signals to base stations (BSs). The numerical analyzes of the results of the eye diagrams showed excellent bit error rate (BER) and quality factor (Q-factor) values, which proved the good performance of the proposed ROF DP-MZM system, for the three encoding formats used, which was able to generate 3-tupling mm-wave for multiple wireless accesses.
Keywords: Radio-over-Fiber. Dual-Parallel Mach-Zehnder Modulator. NRZ. RZ. Gaussian

1. INTRODUCTION

Radio-on-fiber (RoF) technology has been increasingly used to meet the current and future demands of access networks, as it is able to provide low transmission loss, increased bandwidth, immunity to radio frequency (RF) interference, high flexibility and increased coverage, thus being essential to meet the needs of various wireless multimedia services , such as: high-definition television (HDTV), digital multimedia broadcasting (DMB) and three-dimensional TV (3DTV) (Singh and Raghuwanshi 2015; Xu et al. 2014; Wang et al. 2016). Therefore, the RoF type communication system consists of a microwave photonic (MWP) technique, in which the optical signal of a laser is directly or externally modulated in a central station (CS) and is then transmitted through an optical fiber to a photodiode, which produces millimeter waves (mm-Wave) that are sent to a radio with antennas in a base station (BS) , with the aim of allowing access to multiple devices on the wireless network (Sousa et al. 2020; Idowu et al. 2017), through the use of different access technologies, such as: 3G, 4G, 5G, WiFi (IEEE 802.11), Bluetooth (IEEE 802.15.1),

ZigBee (IEEE 802.15.4), UWB (IEE 802.15.3), WiMAX (IEEE 802.16) simultaneously on a single antenna (Das and Zahir 2014; Sharma and Rana 2017; Chen et al. 2017).

Conventional systems designed for RoF technology consists of several disadvantages, such as: limited number of users, undesirable frequencies in the signals (sidebands), non-linearities and poor system quality (Sharma and Rana 2017; Patel and Dalal 2017). However, when compared to other telecommunications systems, RoF offers the following advantages: lower loss of attenuation, better coverage, increased capacity, resistance to RF interference, engineering reduction, lower energy consumption, lower execution cost and project maintenance (Das and Zahir 2014).

Worldwide interoperability for microwave access (WiMAX) technology provides a more useful solution in resolving the telecommunications bottleneck, but according to (Chen et al. 2017) the 5th generation (5G) mobile communications network is the most anticipated, for offering data transmission and reception capacity 1000 times greater than the current cellular phone system, in addition to having a cost-effective deployment and a high level of flexibility that can be exploited by design strategies that activate and move baseband functions on demand according to need (Patel and Dalal 2017; Khorsandi et al 2019), these and other factors have motivated the scientific community to carry out research in this area.

Several approaches to RoF systems for photonic geration of mm-wave have been reported in the literature over the past 20 years. In this sense, Zhu et al. (2013) proposed and demonstrated the RoF system with frequency 12-tupling optical mm-wave generation using an integrated nested MZM. They showed that with the proper adjustment of the direct current polarization voltages of two sub-MZMs, in which they obtained excellent performance results with BER values of 10^{-10} and a power penalty of 0.67dB for the signal transmitted for more than 60Km.

Zhu et al. (2015) proposed and demonstrated a new scheme for the generation of 120GHz mm-wave through a local RF oscillator (LO) with an MZM. With the proper adjustment of the dc bias of the modulator, they achieved frequencies of 12-tupling with an optical sideband suppression ratio (OSSR) greater than 37dB without the use of a filter. They found that both the extinction rate and the phase difference between the two arms of the optical coupler have an influence on the performance of the generated mm-wave.

According to Zhu et al. (2016a), a dual-parallel polarization modulation (DPPolM) was proposed for the generation of 24GHz frequency sextupled microwave signal without the use of a filter. The signal performance was also analyzed in terms of the OSSR and the spurious suppression ratio (RFSSR), through adequate adjustments of the polarization directions, power and phase differences of the modulated optical signals. The results were satisfactory, with an OSSR greater than 31dB and an RFSSR greater than 25dB for a 4GHz microwave signal. Later, in another paper they showed that frequency octupling, sextupling, or quadrupling microwave signal can also be obtained experimentally, through the appropriate adjustments of the polarization state, the modulation index of the serial modulators and the phase of the RF driving signal (Zhu et al. 2016b).

In Muthu and Raja (2016) is shown a new low-cost approach to 16-tupling frequency generation was demonstrated through a 60GHz bidirectional RoF system using

two parallel cascading MZMs. This system simultaneously supported two base stations with bidirectional data transmission between BS and CS through wavelength reuse, so the connection distance can be extended up to 60km with a power penalty of 0.5dB and BER of 10^{-9} for both the upstream signal and the downstream signal.

Gao et al. (2016) experimentally proposed and demonstrated a photonic system using polarization-division multiplexing Mach–Zehnder modulator (PDM-MZM), which simultaneously performed frequency downconversion, multichannel phase shifting, and in-phase (I) and quadrature (Q) demodulation for wideband microwave signals without changing any configuration. They stated that, this system can be easily extended to multichannel applications with independent phase change in each channel and continuously adjusted in the range of 360 degrees. Thus, in the scheme proposed by them, the 40GHz vector signals with various modulation formats were successfully demodulated, thus they stated that this system could potentially be used in other applications, including beam forming, phase detection, phase noise, and Doppler frequency shift Measurement.

Zhu et al. (2017) presented states that with a double polarization modulator in a RoF communication system without a filter, it is possible to generate frequency sextupled microwave signal and achieve suppression of optical sidebands. Thus, by properly adjusting the power ratio of the orthogonal polarization directions, it is possible to cancel two first order sidebands and achieve the pure frequency sextupled signal with an OSSR greater than 38dB and RFSSR greater than 32dB.

Zhou et al. (2018) proposed an ROF system based on the four-wave mixing (FWM) technique, for transmission rate of 2.5Gbps and with RFs of 20GHz, 40GHz and 60GHz, capable of providing frequency multiplication, through the use of a dual-parallel Mach-Zehnder modulator (DP-MZM) in CS and a semiconductor optical Amplifier (SOA) after an SMF with a length of up to 40km. The RoF system presented by them was able to conduct and support multiple mm-wave wireless accesses with excellent performance results.

Alipoor and Sheikhi (2018) studied the nonlinear effects of FWM in a 16-channel dense wavelength division multiplexing radio over fiber (16 - DWDM - RoF) system with direct and external optical double side band (ODSB) modulation. The results of the simulations of this project showed that the external modulation obtained the best performance than the direct modulation in the parameters such as optical signal-to-noise ratio (OSNR), Q-Factor and bit error rate (BER) both in the variation of input power, spacing between channels, bit rate and length of the SMF. Thus, for a RoF system with external ODSB modulation with input power of 10dBm, channel spacing of 100GHz, bit rate of 10Gbps and link of 20km, they obtained Q-factor of about 20 and BER less than 10^{-84}, but for the RoF system with direct modulation the Q-factor was 3.5 and the BER was less than 10^{-4}.

In this paper, we propose the simulation of a RoF DP-MZM system based on nonlinear and dispersive effects through the external modulation technique. Our RoF system was built according to the techniques proposed in Chen et al. 2011; Li et al. 2015; Gao et al. 2016; Alipoor and Sheikhi 2018; and Sousa et al. 2018) where it was able to considerably reduce non-linear and dispersive effects on the link with a distance of up to

80km and signal power of up to 15dBm. The article structure was organized as follows: the theoretical analysis of the modulation technique, the operating principle and the proposed ROF system setup are presented in section 2, the simulations and results analysis are presented in section 3. Finally, the conclusion is presented in section 4.

2. MECHANISM OF THE PROPOSED SYSTEM

2.1 Simulation Setup

Mach-Zehnder modulators (MZM) are opto-electric (OE) converters, which through special techniques may be able to compensate for linearization or dispersion individually or simultaneously. The phase and amplitude relationship between the optical carrier and the new sidebands generated can be tuned according to the phase and amplitude control techniques of the optical carrier, this is, using an integrated polarization-division multiplexing Mach-Zehnder modulator, radio frequency (RF) signals can be frequency downconverted to multichannel intermediate frequency (IF) signals and the phase of each IF signal can be independently and arbitrarily tuned (Gao et al. 2016; Kumar et al. 2016).

Figure 1 shows the conceptual diagram of a DP-MZM, with two sub-MZMs that act on each arm of the main modulator (MZM_c). In its operating principle, the MZM_a is driven by the RF $V_E(t)$ signal and the dc-bias polarization $V_{bias\text{-}a}$ and the MZM_b is driven by the dc-bias polarization $V_{bias\text{-}b}$ and finally a dc-bias polarization $V_{bias\text{-}c}$ controls the phase relationship of the two sub-MZMs, after DP-MZM. Therefore, with this cascade modulator scheme it is possible to achieve the generation of mm-wave of several orders at the signal output, after the DP-MZM. In the simulations, we investigated a simple scheme for the generation of mm-wave, which operates without an electric phase shifter and with an optical filter.

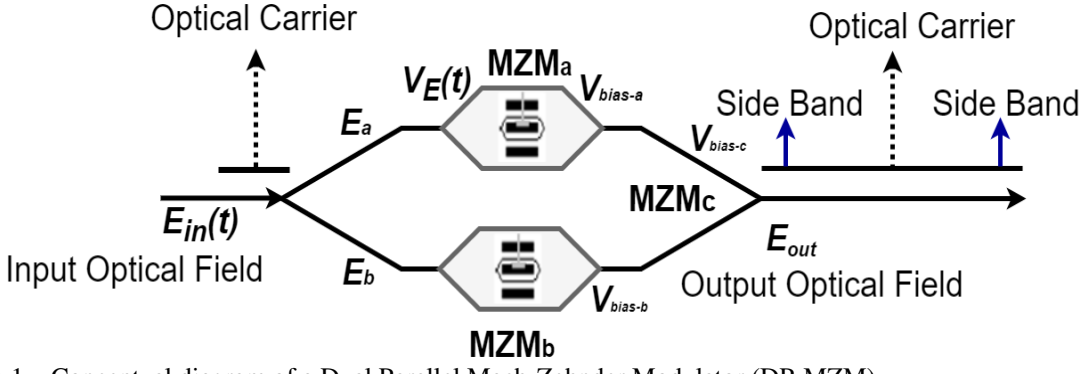

Figure 1 – Conceptual diagram of a Dual Parallel Mach-Zehnder Modulator (DP-MZM).

The used simulation configuration for the verification of the proposed system is shown in Figure 2. An optical carrier given by a continuous wave (CW) laser source $E_{in}(t) = E_0 \exp\{j[\omega_c t + \phi(t)]\}$ was divided equally into the two modulators in parallel (MZM_a and MZM_b) that produced fields such as (Tao et al., 2020):

$$E_a = \sqrt{\gamma}\sum_{n=-\infty}^{\infty}(-1)^n J_{2n}(\beta)\exp[j(\omega_c + 2n\omega)t] + \sqrt{\gamma}(1-2\gamma)\sum_{n=-\infty}^{\infty}(-1)^n J_{2n-1}(\beta)\exp\{j[\omega_c + (2n-1)\omega_m]t + j\frac{\pi}{2}\} \quad (1)$$

and

$$E_b = \left[\sqrt{1-\gamma}\cos\left(\pi\frac{V_{bias-b}}{2V_\pi}\right)\right]\exp(j\omega_c t) + \sqrt{1-\gamma}\cdot(2\gamma-1)\sin\left(\pi\frac{V_{bias-b}}{2V_\pi}\right)\exp\left[\left(\omega_c t+\frac{\pi}{2}\right)j\right] \quad (2)$$

MZM_c is DC biased at V_{bias-c} to introduce a phase difference into the output electrical fields of the MZM_a and the MZM_b. The output of the MZM_c is given by equation 3, disconsidering the side band terms (Tao et al., 2020):

$$E_{out} = E_a + E_b \approx$$

$$\left[\gamma J_0(\beta) + (1-\gamma)\cos\left(\pi\frac{V_{bias-b}}{2V_\pi}\right)\exp\left(j\pi\frac{V_{bias-c}}{V_\pi}\right)\right]\cdot$$

$$\exp(j\omega_c t) + \left[(1-\gamma)(2\gamma-1)\sin\left(\pi\frac{V_{bias}}{2V_\pi}\right)\cdot\exp\left(j\pi\frac{V_{bias-c}}{V_\pi}\right)\right]\cdot$$

$$\exp\left[\left(\omega_c t+\frac{\pi}{2}\right)j\right] - (1-2\gamma)\gamma J_1(\beta)\cdot\left\{\exp\left[j(\omega_c+\omega_m)t + j\frac{\pi}{2}\right] + \right.$$

$$\left.\exp\left[j(\omega_c-\omega_m)t + j\frac{\pi}{2}\right]\right\} - \gamma J_2(\beta)\{\exp[j(\omega_c+2\omega_m)t] +$$

$$[j(\omega_c-2\omega_m)t]\} + (1-2\gamma)\gamma J_3(\beta)\cdot\left\{\exp\left[j(\omega_c+3\omega_m)t + j\frac{\pi}{2}\right] + \right.$$

$$\left.\exp\left[j(\omega_c-3\omega_m)t + j\frac{\pi}{2}\right]\right\} + \gamma J_4(\beta)\{\exp[j(\omega_c+4\omega_m)t] + \exp[j(\omega_c-4\omega_m)t]\} \quad (3)$$

where E_0 is the input field, $\omega_c = 2\pi f_c$ is the angular frequency of the optical carrier, $\phi(t)$ is the phase fluctuation of the optical field, $\beta = \pi V_m / 2V_\pi$ is the modulation index (MI), $V_m = V_{RF}\cos(\omega_m t)$, ω_m are the amplitude and the angular frequency of the RF driving signal, V_π is the half-switch voltage, γ is the power splitting ratio of the DP-MZM, *Jn(·)* is the nth-order Bessel function of the first kind.

Figure 2 presents stage 1 of the proposed RoF DP-MZM system. This system is composed of two sub-Mach-Zehnder Modulators (sub-MZMs) external and they act on each arm of the main modulator, which is called of dual-parallel Mach-Zehnder modulator (DP-MZM). Both sub-MZMs are biased in their maximum transmission point (MATP). The sub-MZMs are triggered by the RF signal sent by the sine generator with frequencies from 20GHz to 80GHz. A Continuous Wave (CW) laser was used as an optical carrier with frequency for the wavelength of 1552.5nm and power from -15dBm to 15dBm at the DP-MZM input. According to this scheme was possible to achieve the generation of 3-tupling mm-wave at the signal output, which are side bands of ±3rd order symmetrically spaced in the frequency domain, below and above the optical carrier.

The output signal of the DP-MZM was coupled by a WDM interleaver Demux and was later sent to stage 2, which is a Mach-Zhender interferometer (MZI) with another Mach-zehnder modulator (MZM_c) in its upper arm. The WDM interleaver Demux had the function of dividing the stage 1 signal for each of the MZI arms. In the upper arm of the MZI, the baseband data with three encoding formats (NRZ, RZ or Gaussian) was added to

the signal for the transmission rate of 10Gbps, which were later modulated by the MZM_c, and then, the optical mm-wave signal and the optical carrier were coupled at the output of the pump coupler co-propaganting and sent to a SMF of up to 80km in length.

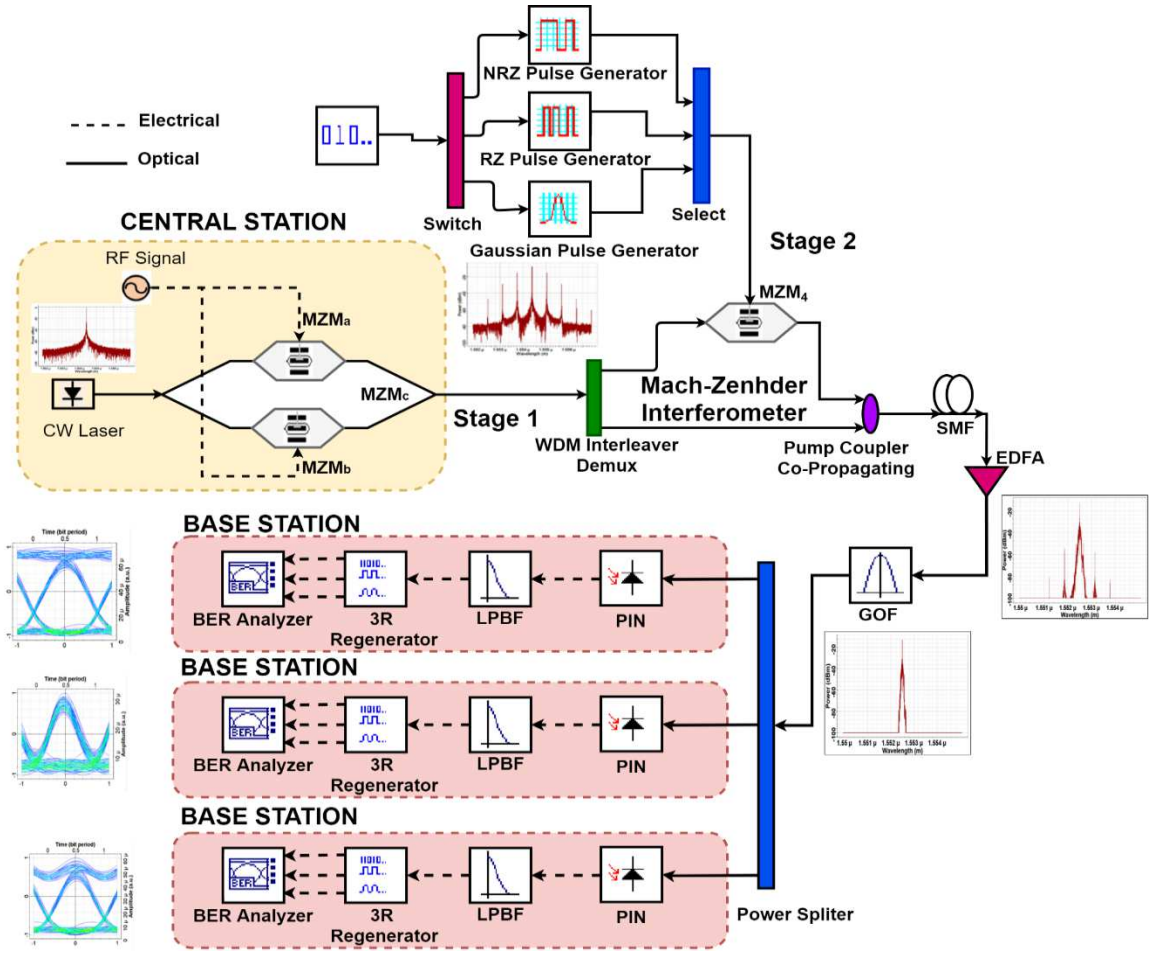

Figure 2 - Schematic of the RoF-DP-MZM system proposed with three coding formats (NRZ, RZ and Gaussian).

The signal composed of the sidebands and the carrier after being transmitted by several kilometers of SMF was amplified by an erbium doped fiber amplified (EDFA) and later a gaussian optical filter (GOF), it was used to reduce the amplified spontaneous emission (ASE) noise emitted by EDFA and, also, to remove the sidebands of the signal and allow the propagation of the optical carrier only.

Then, the optical carrier signal was distributed through a power spliter for each of the BSs. As shown in Fig. 2, the BSs are composed of a Positive Intrinsic Negative (PIN) photodetector that was responsible for converting the optical signal into an electrical signal and a low pass Bessel filter that was used to remove noise in the electrical signal. The performance analysis of the RoF DP-MZM system was performed according of the eye diagram which provides BER and Q-factor values through the use of BER analyzer at the signal output in each of the BSs.

3. NUMERICAL SIMULATION RESULTS AND DISCUSSION

In this work, the MATLAB and OptiSystem softwares were used to simulate and to analyze the performance of the RoF-DP-MZM scheme with three coding signals: Non-Return-to-Zero (NRZ), Return-to-Zero (RZ) and Gaussian, which are shown through the graphs of pulse formats and eye diagrams in Figures 3 and 4, respectively. In the simulations, the three types of coding were used alternately according to the simulation parameters tabulated in Table I. The analysis of the system performance of the system for the transmission rate of 10Gbps was performed through the results collected from the optical spectrum and the eye diagram as a function of the variation of the following parameters: mm-wave frequencies from 20GHz to 80GHz, input power from -15dBm to 15dBm and the fiber length from 0km to 80km.

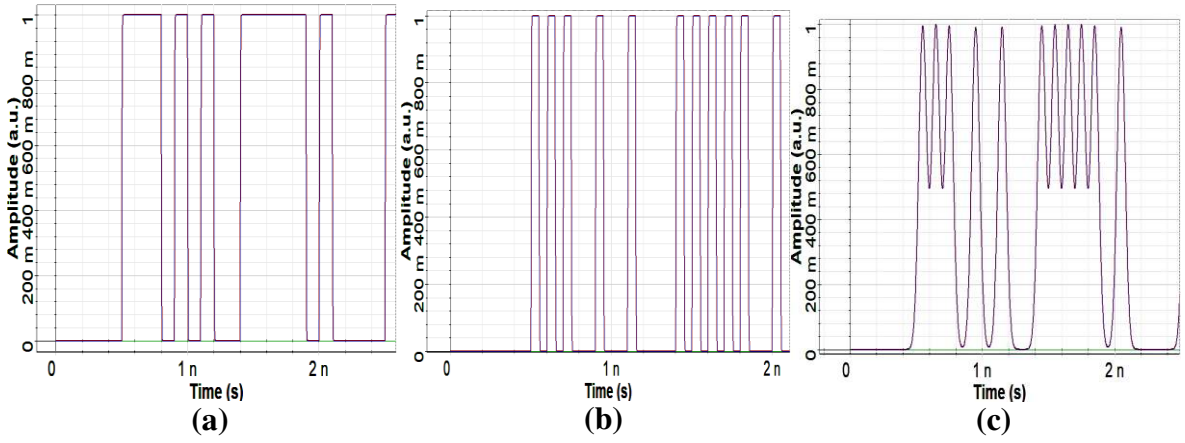

Figure 3 - (a) NRZ pulse, (b) RZ pulse and (c) Gaussian Pulse.

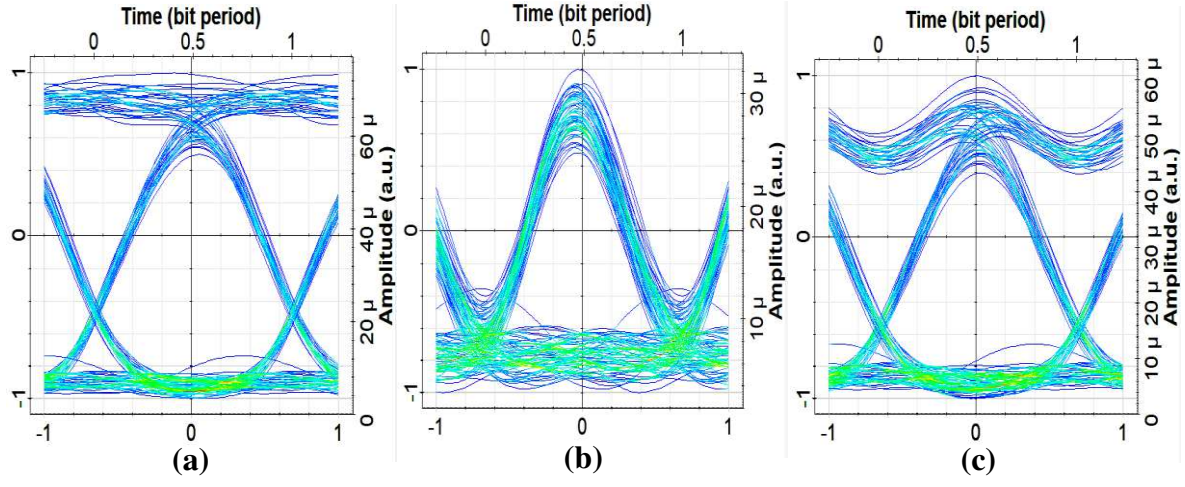

Figure 4 - Eye diagram of the received signal for 20GHz mm-wave and for pulse formats NRZ (a), RZ (b) and Gaussian (c).

The performance analysis of digital transmission systems through the eye diagram has been considered a simple and powerful technique (Agrawal 2012), which is also convenient for the study of the effects of intersymbol interference (ISI) and losses in signal quality due to dispersion and non-linearities. Thus, through the study of the eye diagram it

is possible to visualize distortions in the shape of the received signal and extract various useful information, such as: height of eye opening, timing jitter, noise level, bit error rate (BER) and quality factor (Q-Factor). The results of these parameters have been widely used for the analysis of fiber optic communication systems in several related studies (Singh and Raghuwanshi 2015; Xu et al 2014; Sousa et al 2018; de Sousa et al. 2020; Venkatral and Prashanth 2018), but the proposed RoF system analysis was performed only through the Q-factor and BER.

Figure 5(a) shows the optical spectrum graph of the CW laser output (optical carrier) with a central frequency of 1552.5nm and an input power of 0dBm. In Figures 5(b) and 5(c), the graphs of the spectra of the signal output after the DP-MZM are shown for the mm-wave frequencies of 20GHz and 80GHz, respectively. We highlight that the data were collected for the variation of mm-wave frequencies of 20GHz, 40GHz, 60GHz and 80GHz, but for reasons of organization of this paper, we prefer to present initially the optical spectra only for the cases with mm-wave frequencies of 20GHz and 80 GHz, which are sufficient to show the effects that occur in the signal depending to the variation of the mm-wave frequency.

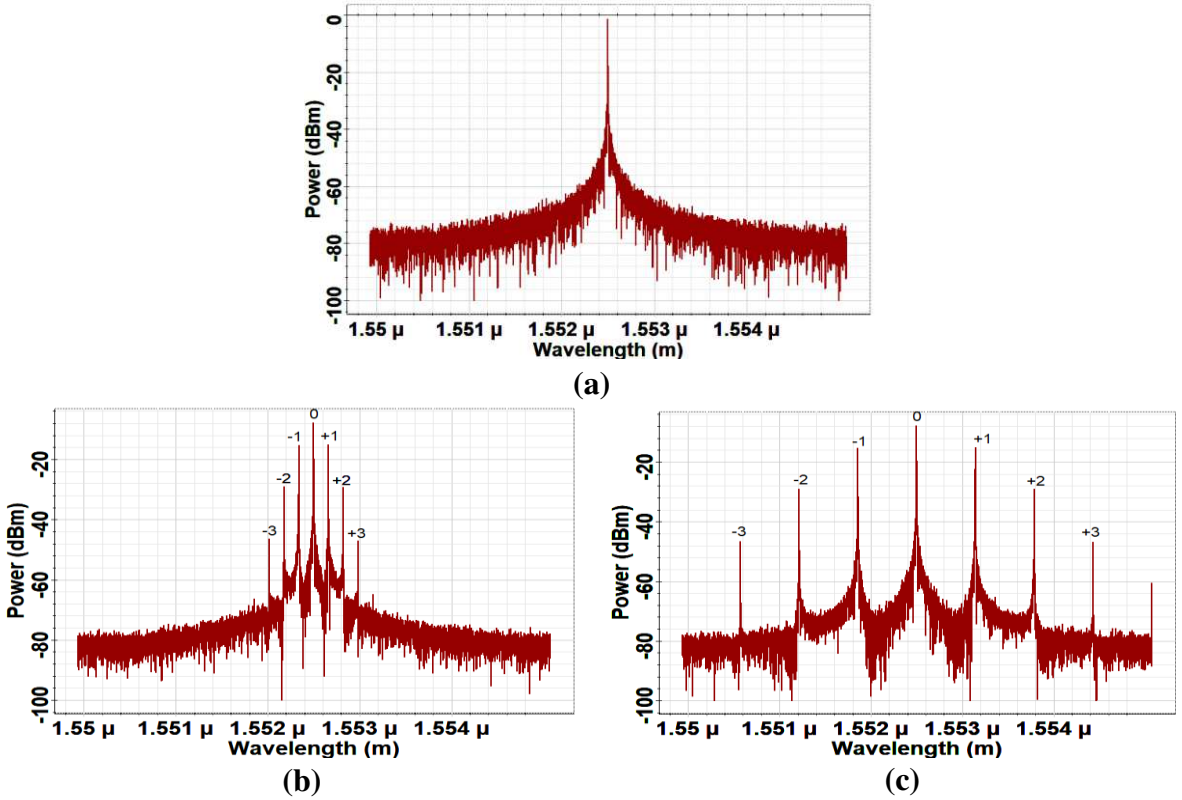

Figure 5 - Transmitted signal at BS: Output Spectrum of the CW Laser (carrier) (a) and Spectra periodic optical sidebands at the DP-MZM output for the mm-wave frequency equal to 20 GHz (b) and 80 GHz (c), respectively.

In the spectra of Figures 5(b) and 5(c) can be observed the presence of symmetrical side bands downstream (1552nm, 1552.2nm, 1552.3nm, 1552.7nm, 1552.8nm and 1553nm) with the optical carrier (1552.5nm). These symmetrical side bands are harmonic up to ±3rd order, with wavelengths and powers that are presented neatly in table II, where it

is possible to observe an increase in the spacing between the side bands and the optical carrier, when the frequency of mm-wave was increased of 20GHz to 80GHz.

Table II – Wavelengths and Powers of Downstream Sidebands.

Nº	RF Frequencies							
	20GHz		40GHz		60GHz		80GHz	
	Wavelength (nm)	Power (dBm)	Wavelength (nm)	Power (dBm)	Wavelength (nm)	Power (dBm)	Wavelength (nm)	Power (dBm)
-3	1552	-46.5	1551.6	-46.4	1551	-46.5	1550.6	-46.7
-2	1552.2	-28.9	1551.8	-29	1551.5	-28.9	1551.2	-28.9
-1	1552.3	-15.2	1552.2	-15.5	1552	-15.6	1551.9	-15.2
0	1552.5	-7.9	1552.5	7.5	1552.5	-8	1552.5	-7.9
1	1552.7	-15.2	1552.8	-15.5	1553	-15.6	1553.1	-15.2
2	1552.8	-28.9	1553.2	-29	1553.5	-28.9	1553.8	-28.9
3	1553	-46.5	1553.4	-46.4	1554	-46.5	1554.4	-46.7

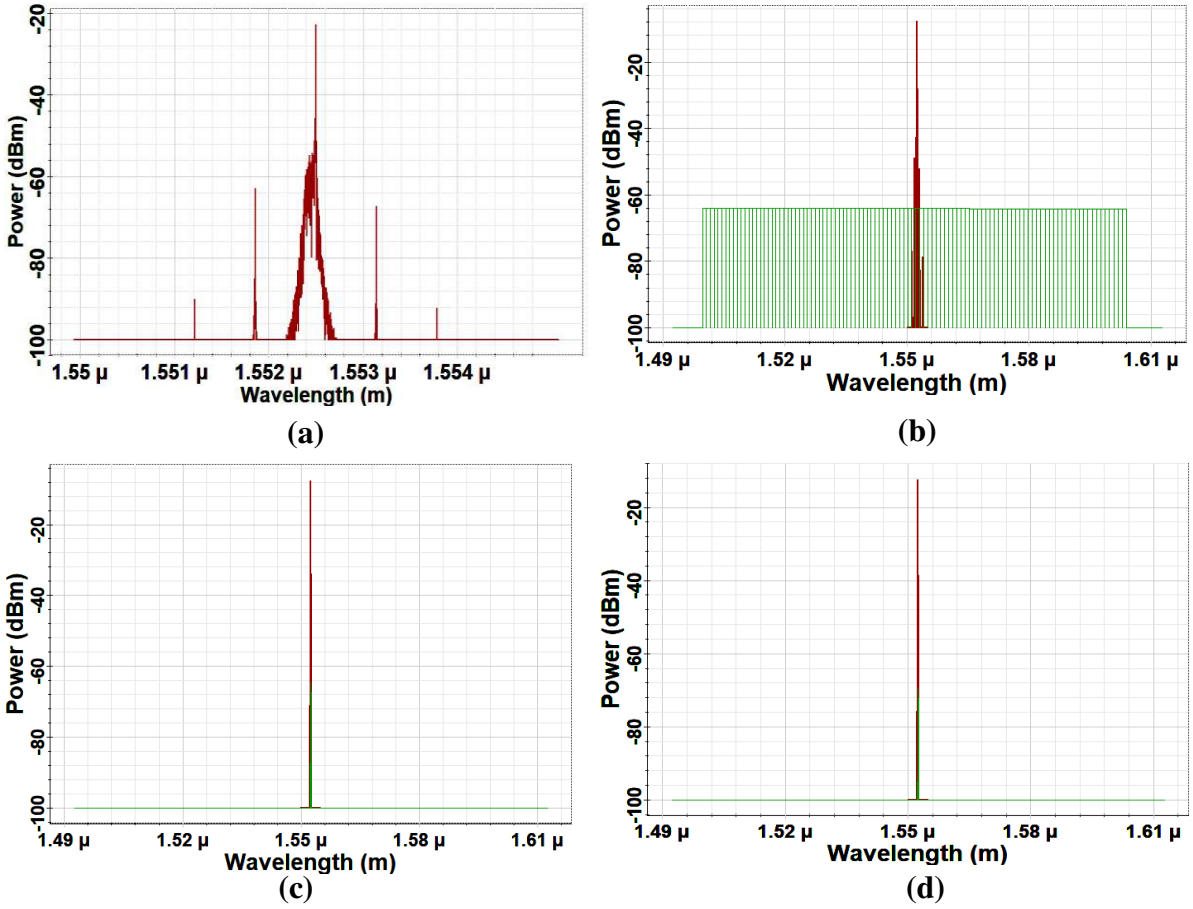

Figure 6 – Optical Signal Spectrum at the WDM interleaver Demux (a), EDFA (b) GOF (c) and of BSs (d) outputs.

After the signal transmission through the WDM interleaver Demux, part of the side bands was suppressed, leaving only the optical carrier and the side bands, which were later sent to the SMF. As shown by the results of the optical signal spectrum after WDM interleaver Demux in Figure 6(a), a power value of -22.9dBm was obtained for the optical

carrier and for the sidebands of -3rd order (1552nm) and +3rd order (1553nm), powers equal to -63dBm and -67.3dBm, respectively.

Figure 6(b) shows the optical spectrum amplified by EDFA, which performed a process of amplification and gain of optical signal power. In this optical spectrum there is still the presence of the side bands together with the optical carrier and ASE noise. Subsequently, the side bands were suppressed by GOF as shown by the optical spectrum of the signal in Figure 6(c). As was observed in the numerical simulations, the suppression of the side bands of ±3rd order occurred regardless of the SMF length and the mm-wave frequency, in the three pulse formats proposed. Therefore, the signal arrived at the base stations (BS_1, BS_2 and BS_3) without the presence of side bands and with power of approximately -17dBm, as shown in Figure 6(d).

3.1 Fiber Length Effects

The performance analysis of the communication link for the transmission rate of 10Gbps and input power of 0dBm, was carried out through the eye diagrams of the downstream data of 20GHz, 40GHz, 60GHz and 80GHz, after the SMF with 0km (B-T-B), 20km, 40km, 60km and 80km, for the power of the 0dBm CW laser with RZ, NRZ and Gaussian encoding, which are shown in Figures 7(a), 7(b), 7(c) and 7(d), respectively. Through the results obtained, it was possible to observe that due to the increase of the non-linear effects, dispersion and attenuation in the signal transmission, the performance of the proposed RoF system was reduced, because the quality factor decreased and consequently, the bit error rate increased as the length of the SMF increased. Therefore, for all cases, the best performance occurred for the 20km fiber and the worst performance was found for the 80km fiber, this can also be seen through the eye diagrams in Figures 8, 9 and 10.

In the obtained results was possible to note that in most cases the RoF DP-MZM scheme with NRZ encoding obtained better tolerance to dispersion, to nonlinear effects and to the noise manifested with the increase in SMF length, consequently the best transmission performance results were obtained, that is, higher quality factor values and lower bit error rate values , when compared to the RoF DP-MZM schemes with RZ and Gaussian encoding, according to the Q-Factor graphs versus transmission distance for the signal received in the BSs, shown in Figures 7(a), 7(b), 7(c) and 7(d).

In the eye diagrams of Figures 8, 9 and 10, the red color graph represents the BER value as a function of the SMF length for each encoding format used, both for 80GHz downstream data. Thus, for the RoF DP-MZM system with NRZ encoding format the Q-Factor values obtained for 20km, 60km and 80km were: 15.5957, 12.7422 and 7.42646, respectively. Similarly, the BER values obtained for 20km, 60km and 80km were: 3.83014×10^{-55}, 1.72215×10^{-37}, 5.52838×10^{-14}, respectively (Figure 8). For the RoF DP-MZM system with RZ encoding format, the Q-Factor values obtained for 20km, 60km and 80km were: 12.9256, 3.46564 and 2.63623, respectively. Similarly, the BER values obtained for 20km, 60km and 80km were: 1.3792×10^{-38}, 0.000264215, 0.00364023, respectively (Figure 9). And for the RoF DP-MZM system with Gaussian encoding format the Q-Factor values obtained for 20km, 60km and 80km were: 11.2757, 9.39981 and 5.56815, respectively. Similarly, the BER values obtained for 20km, 60km and 80km were: 8.47293×10^{-30}, 2.7279×10^{-21}, 1.28668×10^{-8}, respectively (Figure 10).

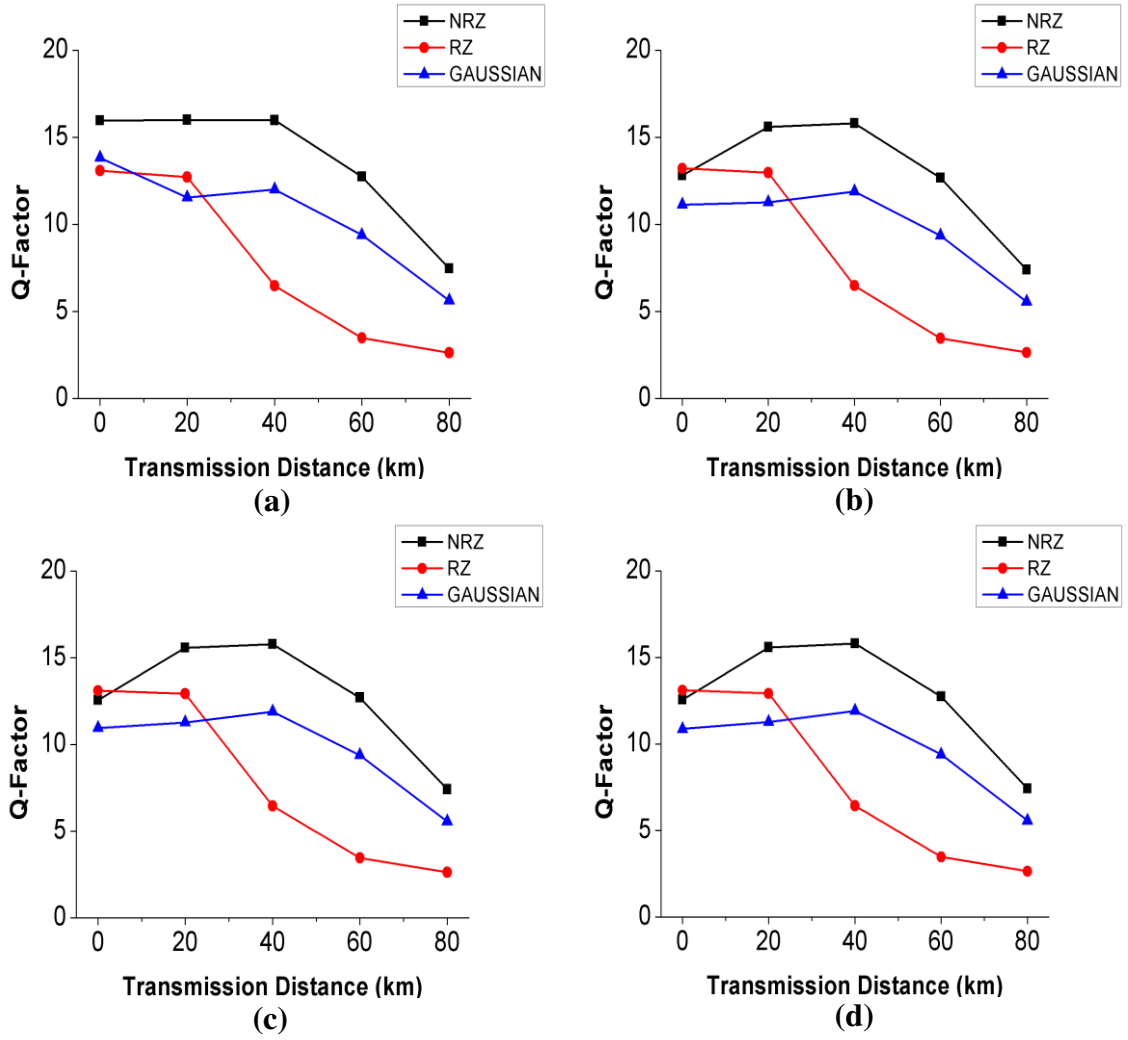

Figure 7 – Q-Factor versus transmission distance for Downstream data of 20GHz (a), 40GHz (b), 60GHz (c) and 80GHz (d) for baseband signals with NRZ, RZ and Gaussian encoding.

Thus, the eye diagrams of Figures 8, 9 and 10 show that for the three encoding formats used in the proposed RoF DP-MZM system, that there was also a reduction in the height and amplitude of the eye diagram as the length of the SMF increased, mainly for the RoF system with 80km SMF, where it was possible to clearly observe that the eye diagrams are stressed, mainly for the RoF DP-MZM system with RZ encoding format. In this sense, the RoF DP-MZM system with RZ encoding format had a greater performance reduction from 60km to 80km of SMF, as shown by the eye diagrams of Figures 9(b) and 9(c), when compared with the RoF DP-MZM systems with NRZ coding in Figures 8(b) and 8(c) and with Gaussian coding, presented in Figures 10(b) and 10(c).

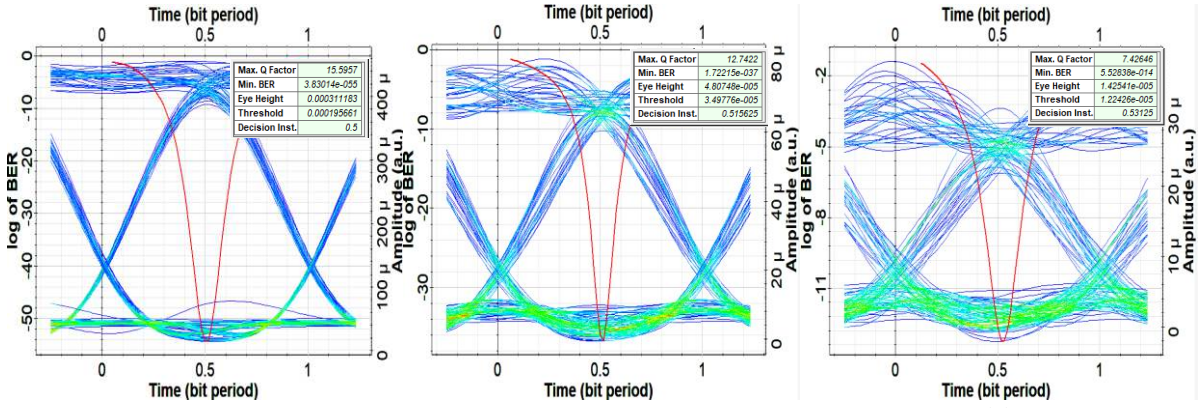

(a) (b) (c)

Figure 8 - Eye diagram for the proposed RoF system with (a) 20km and (b) 60km and (c) 80km, both for 80GHz downstream data of NRZ encoding.

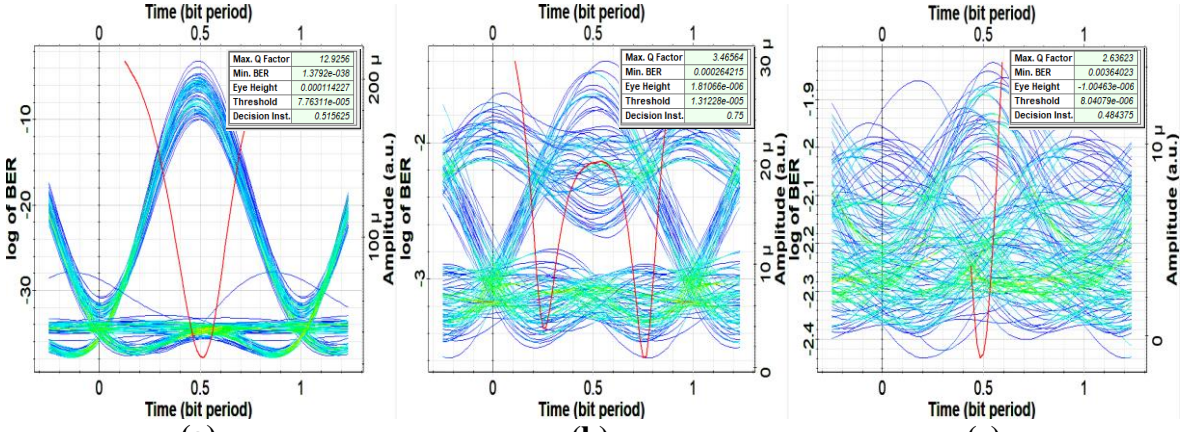

(a) (b) (c)

Figure 9 - Eye diagram for the proposed RoF system with (a) 20km, (b) 60km and (c) 80km, both for RZ encoding 80GHz downstream data.

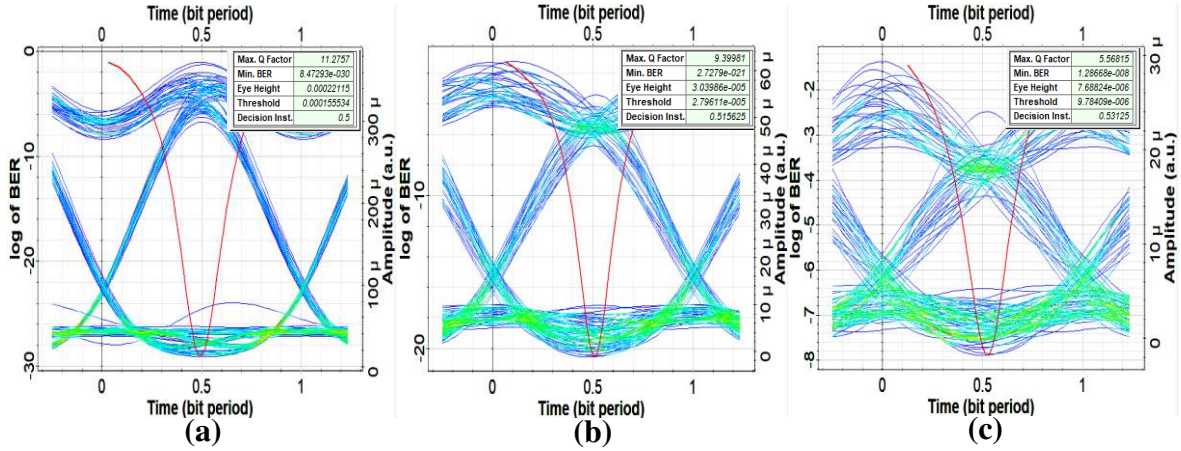

(a) (b) (c)

Figure 10 - Eye diagram for the proposed RoF system with (a) 20km, (b) 60 km and (b) 80km, both for 80GHz downstream gaussian encoding data.

3.2 Input Power Effects

Figure 11 shows the log BER versus Input Power graphs, where the signal power was varied from -15dBm to 15dBm for the mm-wave frequencies varied from 20GHz to 80GHz and also for each of the baseband signals with Non-Return-to-Zero (NRZ), Return-to-Zero (RZ) and Gaussian encodings. In the simulations it was noticed that with the increase of the input signal power the non-linear and dispersive effects increased resulting in undesirable distortions in the signal, which reduced the quality factor and increased the bit error rate, therefore, consequently the proposed RoF schemes had reduced performance for the three types of encoding signals used.

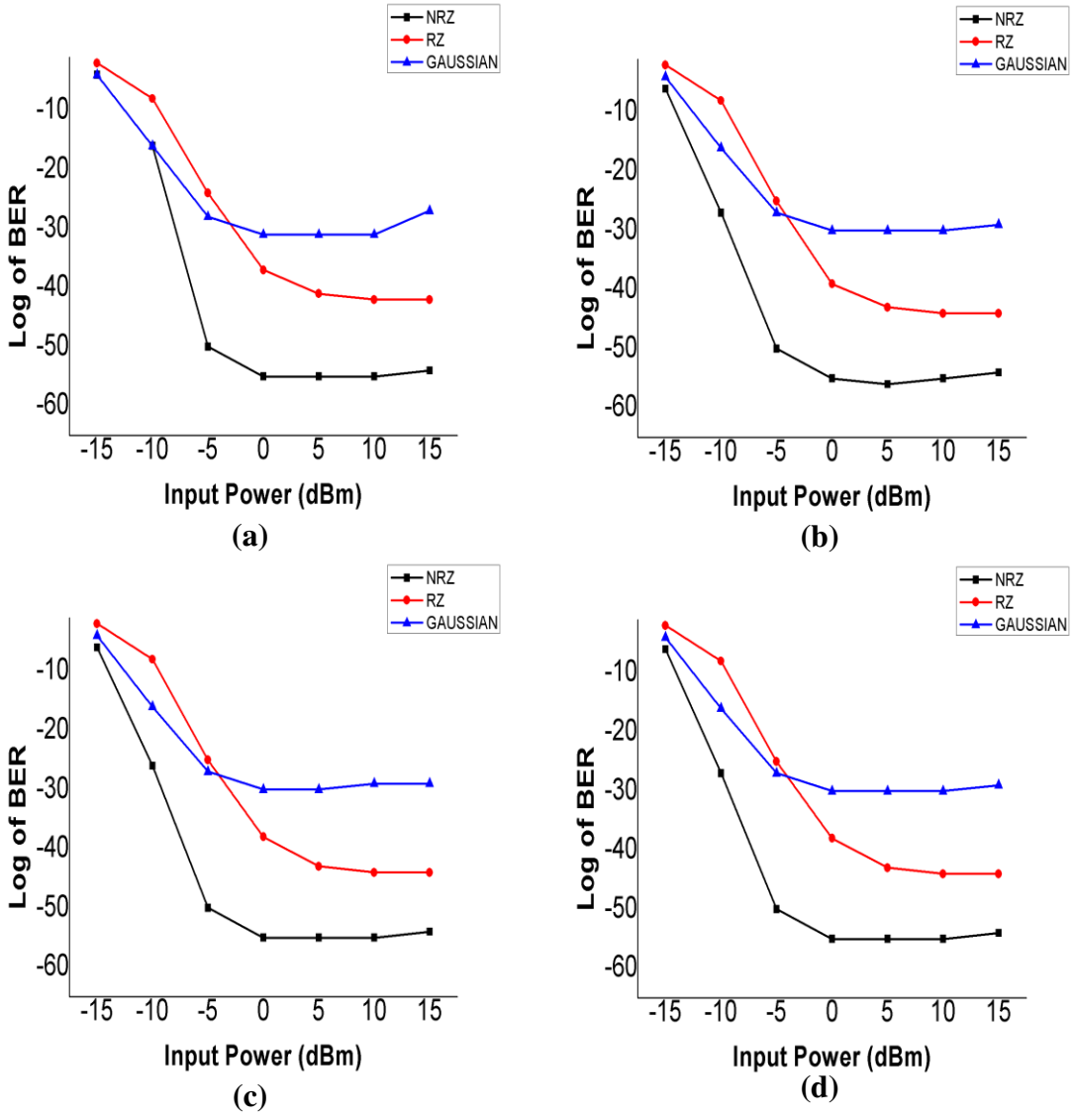

Figure 11 - Log BER versus Input Power for Downstream data of 20GHz (a), 40GHz (b), 60GHz (c) and 80GHz (d) for baseband signals with NRZ, RZ and Gaussian coding.

The Log BER behavior with Input Power (Figure 11) is due to in any fiber optic communication system the Q-factor value should be as high as possible up to a certain threshold for an optimal power value of the transmitted signal. In this sense, for low power levels the performance of the system is limited by undesirable noises, while for high power levels the system performance is reduced by non-linear effects. Another fact is that during the process of data transmission in SMF, various nonlinear and dispersive effects can induce power variations, which also affect system performance according to transmission time (Agrawal, 2012).

According to the graphs of log BER versus the input power signal, which are shown in Figures 11(a), 11(b), 11(c) and 11(d), it was possible to observe that in most cases, again the RoF scheme with NRZ encoding obtained better tolerance to dispersion, non-linear effects and noises, which were manifested with the increase in signal power. Thus, the best results of signal transmission performance were obtained, that is, higher values of the quality factor and lower bit error rate values were obtained, when compared to RoF schemes with RZ and Gaussian encoding. This can also be seen through the eye diagrams shown in Figures 12, 13 and 14, in which the red color graphs represent the Q-factors values as a function of the variation of the input signal power of -15dBm, 0dBm and 15dBm for each encoding format used, both for 80GHz downstream data.

Thus, for the RoF system with NRZ encoding format, the Q-Factor values obtained for -15dbm, 0dBm and 15dBm were: 4.5286, 16.0638 and 15.9194, respectively. Similarly, the values obtained from BER were: 2.96085×10^{-6}, 2.24129×10^{-58}, 2.27664×10^{-57} (Figure 12). For the RoF system with RZ encoding format, the Q-Factor values obtained for -15dbm, 0dBm and 15dBm were: 2.02644, 12.7328 and 13.531, respectively. Similarly, the values obtained from the BER were: 0.0213597, 1.64137×10^{-37}, 4.24391×10^{-42} (Figure 13). And for the RoF system with Gaussian encoding format, the values obtained from the Q-Factor for the input power -15dBm, 0dBm and 15dBm were: 3.46999, 11.5584 and 11.3665, respectively. Similarly, the values obtained from BER were: 0.000260192, 3.26753×10^{-31}, 2.9895×10^{-30} (Figure 14).

Therefore, the eye diagrams of Figures 12, 13 and 14 show that for the three encoding formats used in the proposed RoF system, there was an increase in the Q-factor and a reduction in the BER up to a certain threshold as the input signal power increased. However, from the power limit of each of the proposed RoF systems, there was a reduction in the height and amplitude of the eye diagram as the input power of the signal was increased up to 15dBm, this can be seen clearly in the eye diagrams in the Figures 12(c), 13(c) and 14(c). It is also noteworthy that for RoF systems with input power of -15dBm, the eye diagrams are considerably stressed, this was due to the limitation of the systems to the noises that manifested during the signal transmission process, which resulted in low performance for the three types of encoding used for 80GHz downstream data, however this effect also occurred with the other mm-Wave frequencies used as shown in the graphs of Figure 11.

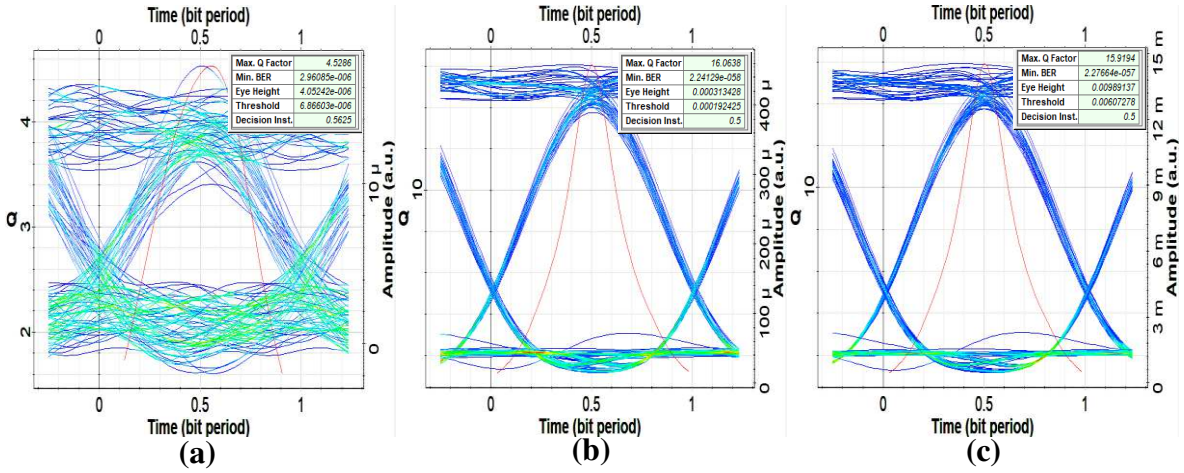

Figure 12 - Eye diagram at, (a) -15dBm input power, (b) 0dBm input power and (c) 15dBm input power for the Non-Return-to-Zero (NRZ) coding signals.

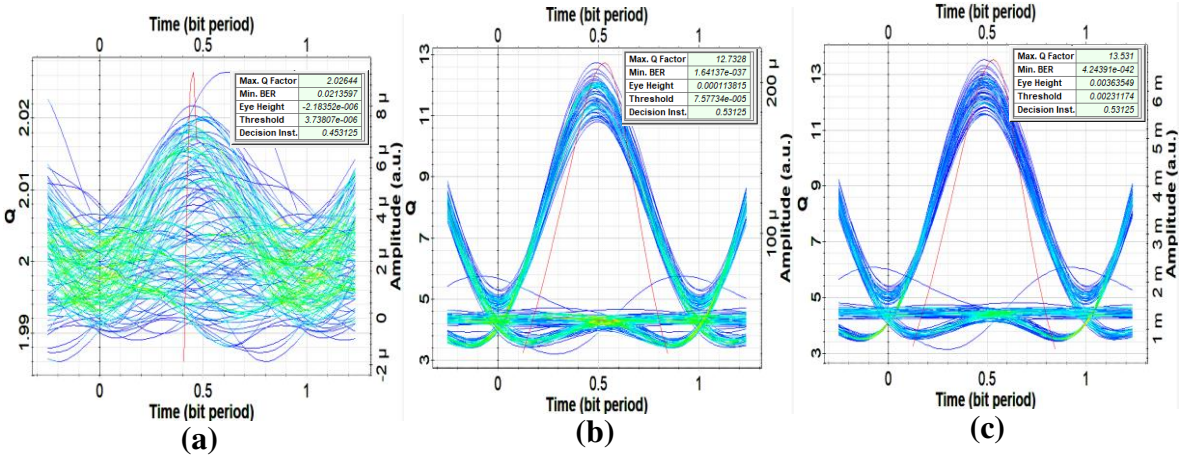

Figure 13 - Eye diagram at, (a) -15dBm input power, (b) 0dBm input power and (c) 15dBm input power for the Return-to-Zero (RZ) coding signals.

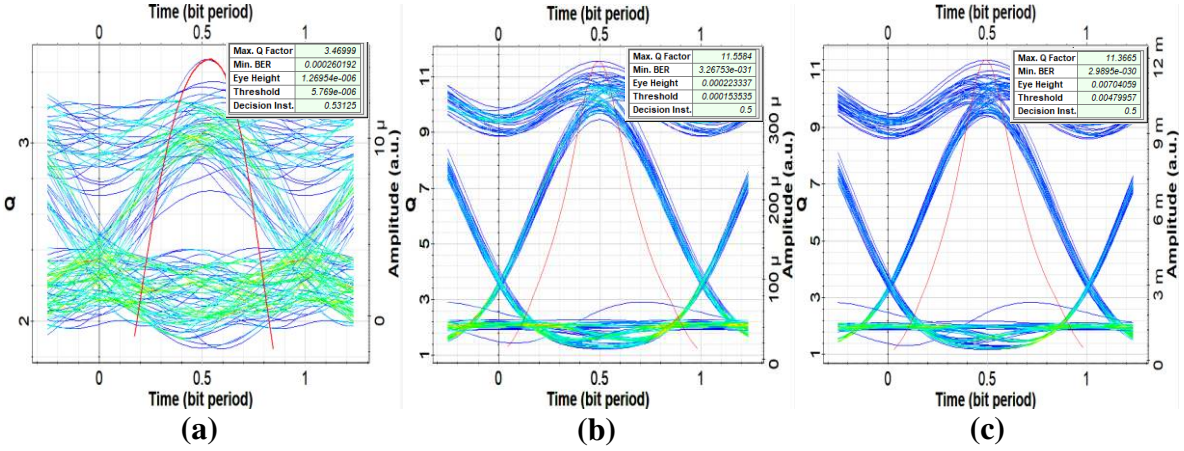

Figure 14 - Eye diagram at, (a) -15dBm input power, (b) 0dBm input power and (c) 15dBm input power for the Gaussian encoding signals.

4. CONCLUSION

The proposed RoF DP-MZM system was numerically demonstrated, which was able to satisfactorily generate ±3rd order mm-wave for the purpose of providing multiple multiband wireless accesses in the various BSs, at a transmission rate of 10Gbit/s and RF frequencies of 20GHz, 40GHz, 60GHz and 80GHz. The system performance was investigated through signal power and SMF length. The results showed the Q-factor value and the eye diagram were excellent for the three coding formats used, especially the NRZ, which obtained better performance values both for the variation of the SMF length and in the variation of the signal power. Therefore, the proposed RoF system can be considered of simple structure and suitable for the implementation of modern wireless communication systems in the presence of non-linear and dispersive effects.

ACKNOWLEDGMENTS

This study was financed in part by the Coordenação de Aperfeiçoamento de Pessoal de Nível Superior – Brasil (CAPES) – Finance Code 001. The authors gratefully acknowledge financial support from PROPESP/UFPA. The author W.Paschoal Jr. gratefully acknowledge supporting from FACIN/UFPA, FACFIS/UFPA, PPGF/UFPA, ICEN/UFPA, PROEG/UFPA, NanoJovem/PROEX/UFPA, PIBID/CAPES, and the Brazilian agencies FINEP, CAPES and MAI/MCTIC/CNPq.

ORCID iDs

Fabio Barros de Sousa ---------- https://orcid.org/0000-0003-4170-5261

Fiterlinge Martins de Sousa ---------- https://orcid.org/0000-0003-3977-5762

Igor Ramon Sinimbú Miranda ---------- https://orcid.org/0000-0001-5229-2701

Waldomiro Paschoal Jr ---------- https://orcid.org/0000-0002-2348-1244

Marcos Benedito Caldas Costa ---------- https://orcid.org/0000-0003-1569-1249

5. APPENDIX

Table I shows the used components parameters in the simulation of the proposed RoF-DP-MZM system, which they were indispensable for the construction of this optical network project.

Table I - Used simulation parameters in the proposed RoF system.

Transmitter Parameters	Value
Sine Generator frequency	20GHz to 80GHz
Sine Generator phase	90 deg
CW laser power	-15dBm to 15dBm
CW laser frequency	1552.5nm
CW laser line width	10MHz
MZM extinction ratio	20dB
MZM Symetrical factor	-1
Power Combiner Number of input ports	2
Power Combiner Loss	0dB

Mach-Zehnder Interferometer Parameters	Value
WDM Interleaver Demux Frequency	1552.5nm
WDM Interleaver Demux Frequency spacing	10GHz
WDM Interleaver Demux Bandwidth	0.06nm
WDM Interleaver Demux Insertion loss	1dB
MZM extinction ratio	20dB
MZM Symetrical factor	-1
Pump Coupler Co-Propagating Signal attenuation	3dB
Pump Coupler Co-Propagating Pump attenuation	0dB
Stage 2 Parameters	**Value**
Pseudo-Random Bit Sequence Generator Bit rate	10e9Bits/s
Pseudo-Random Bit Sequence Generator Operation mode	Order
Pseudo-Random Bit Sequence Generator Operation Order	log(Sequence length)/log(2)
Pseudo-Random Bit Sequence Generator Number of leading zeros	(Time window * 3 / 100) * Bit rate
Pseudo-Random Bit Sequence Generator Number of trailing zeros	(Time window * 3 / 100) * Bit rate
NRZ and RZ Pulse Generators Rectangle shape	Exponential
NRZ and RZ Pulse Generators Amplitude	1a.u.
NRZ and RZ Pulse Generators Bias	0a.u.
NRZ and RZ Pulse Generators	0bit
NRZ and RZ Pulse Generators Rise time	0.05bit
NRZ and RZ Pulse Generators Fall time	0.05
Gaussian Pulse Generators Amplitude	1a.u.
Gaussian Pulse Generators Bias	0a.u.
Gaussian Pulse Generators Width	0.5bit
Gaussian Pulse Generators Position	0bit
Gaussian Pulse Generators Order	1
Link Parameters	**Value**
SMF Attenuation	0.17dB/km
SMF Dispersion	17.8ps/nm/km
SMF Dispersion slope	$0.08ps/nm^2/km$
SMF Effective area	$80\mu m^2$
Length	0 to 80km
EDFA Gain	12dB
EDFA Noise Figure	4dB
GOF Frequency	1552.5nm
GOF Bandwidth	13GHz
GOF Insertion loss	0dB
Receiver Parameters	**Value**
PIN responsitivity	1A/W
PIN Dark current	10Na
PIN Thermal noise	$10^{-21}W/Hz$
Low Pass Bessel Filter Cut off frequency	0.75 * Bit rate Hz
Low Pass Bessel Filter Insertion loss	0dB
Low Pass Bessel Filter Order	4
Bit Rate	10Gbits/s
Sweep Iteration	4

6. REFERENCIES

Agrawal, G. P.: Fiber-optic communication systems (Vol. 222). John Wiley & Sons (2012)

Aldhaibani, A. O., Yaakob, S., Shaddad, R. Q., Idrus, S. M., Kadir, M. A., & Mohammad, A. B.: 2.5 Gb/s hybrid WDM/TDM PON using radio over fiber technique. Optik-International Journal for Light and Electron Optics, **124** (18), 3678-3681 (2013)

Alipoor, A., Mir, A., and Sheikhi, A.: Study of DWDM-ROF link nonlinear effects using direct and external ODSB modulation formats. Journal of Optics. **47**(3), 263-271 (2018)

Arya, R., and Zacharias, J.: Performance improved tunable millimeter-wave signal generation employing UFBG based AOTF with bit walk-off effect compensation. Microwave and Optical Technology Letters. **61**(5), 1221-1230 (2019)

Chen, Y., Wen, A., Guo, J., Shang, L., and Wang, Y.: A novel optical mm-wave generation scheme based on three parallel Mach–Zehnder modulators. Optics Communications. **284**(5), 1159-1169 (2011)

Chen, S., Deng, L., Ye, Y., Chen, X., Cheng, M., Tang, M., and Liu, D.: Experimental Investigation on Improved Predistortion Circuit for Directly Modulated Radio Over Fiber System. IEEE Photonics Journal. **9**(5), 1-9 (2017)

Das, S., and Zahir, E.: Modeling and performance analysis of rof system for home area network with different line coding schemes using optisystem. international journal of multidisciplinary sciences and Engineering. **5**(6), 1-8 (2014)

Gao, Y., Wen, A., Tu, Z., Zhang, W., and Lin, L.: Simultaneously photonic frequency downconversion, multichannel phase shifting, and IQ demodulation for wideband microwave signals. Optics letters. **41**(19), 4484-4487 (2016)

Idowu, P. O., Samuel, O. W., Asogbon, M. G., Wajeed, W. B., and Akinmoladun, T. M.: A Novel Transmission System using Broadband Fiber Optic link for Remote Antenna. Int. J. of Multidisciplinary and Current research. **5**, 299-309 (2017)

Kumar, A. S., Mohan, A. S., Anju, B., Babu, A. S., Jose, J., and Vijayan, M. Performance Analysis of OFDM Based RoF System. International Journal of Scientific & Engineering Research. Vol. **7**, Issue 4, 362–366 (2016)

Li, X., Zhao, S., Zhu, Z., Gong, B., Chu, X., Li, Y., and Liu, Y.: An optical millimeter-wave generation scheme based on two parallel dual-parallel Mach–Zehnder modulators and polarization multiplexing. Journal of Modern Optics. **62**(18), 1502-1509 (2015)

Khorsandi, B. M., Tonini, F., and Raffaelli, C.: Centralized vs. distributed algorithms for resilient 5G access networks. Photonic Network Communications. **37**(3), 376-387 (2019)

Muthu, K. E., and Raja, A. S. Bidirectional MM-Wave Radio over Fiber transmission through frequency dual 16-tupling of RF local oscillator. Journal of the European Optical Society-Rapid Publications. **12**(1), 1-9 (2016)

Patel, D., and Dalal, U. D.: A novel wavelength reused bidirectional RoF-WDM-PON architecture to mitigate reflection and Rayleigh backscattered noise in multi-Gb/s m-QAM

OFDM SSB upstream and downstream transmission over a single fiber. Optics Communications. **390**, 26-35 (2017)

Sharma, A., and Rana, S.: Comprehensive study of radio over fiber with different modulation techniques–a review. International Journal of Computer Applications. **170**(4), 22-25 (2017)

Singh, M., and Raghuwanshi, S. K.: Effect of higher order dispersion parameters on optical millimeter-wave generation using three parallel external optical modulators. Journal of Applied Physics. **117**(2), 023116, 1-10 (2015)

Sousa, F. B., Sousa, F. M., Oliveira, J. E. D., Oliveira, J. M., Paschoal, W., and Costa, M. B.: All-Optical 3R Regeneration Based on an Acousto Optical Filter with Q-Factor Improvement. Journal of Computational and Theoretical Nanoscience, 15(6-7), 1871–1875. (2018)

Sousa, F. M., de Sousa, F. B., Miranda, I. R., Oliveira, J. E., Paschoal Jr, W., and Costa, M. B.: Graphene patch antenna with lateral edges defined by armchair or zigzag structures and PBG substrate. Journal of Computational Electronics. 1-9 (2020)

Tao, L. B., Gao, H. Y., Deng, S., Lü, H. F., Wen, X. Y., & Li, M. A simplified optical millimeter-wave generation scheme based on frequency-quadrupling. Optoelectronics Letters, 16(1), 7-11 (2020).

Xu, K., Wang, R., Dai, Y., Yin, F., Li, J., Ji, Y., and Lin, J.: Microwave photonics: radio-over-fiber links, systems, and applications. Photonics Research. **2**(4), B54-B63 (2014)

Wang, Y., Pei, L., Li, J., and Li, Y.: All optical multi-wavelength single-sideband modulated WDM radio-over-fiber systems by introducing a Sagnac loop filter. Optical Fiber Technology. **32**, 36-42 (2016)

Wang, Y., Pei, L., Li, J., and Li, Y.: Millimeter-wave signal generation with tunable frequency multiplication factor by employing UFBG-based acousto-optic tunable filter. IEEE Photonics Journal. **9**(1), 1-10 (2017)

Zhou, H., Shen, Y., Chen, M., Cheng, J., and Zeng, Y.: A ROF Access Network for Simultaneous Generation and Transmission Multiband Signals Based on Frequency Octupling and FWM Techniques. Advances in Condensed Matter Physics. 1-9 (2018)

Zhu, Z., Zhao, S., Li, Y., Chu, X., Wang, X., & Zhao, G.: A Radio-over-Fiber System with Frequency 12-tupling Optical Millimeter-wave Generation to Overcome Chromatic Dispersion. IEEE Journal of Quantum Electronics, 49(11), 919-922 (2013)

721 Zhu, Z., Zhao, S., Li, Y., Chen, X., & Li, X.: A novel scheme for high-quality 120 GHz
722 optical millimeter-wave generation without optical filter. Optics & Laser Technology, 65,
723 29-35 (2015)

724 Zhu, Z., Zhao, S., Tan, Q., Liang, D., Li, X., & Qu, K.: Photonically assisted microwave
725 signal generation based on two cascaded polarization modulators with a tunable
726 multiplication factor. IEEE Transactions on Microwave Theory and Techniques, 64(11),
727 3748-3756 (2016)

728 Zhu, Z., Zhao, S., Li, X., Qu, K., & Lin, T.: Photonic generation of frequency-sextupled
729 microwave signal based on dual-polarization modulation without an optical filter. Optics &
730 Laser Technology, 87, 1-6 (2017)

731 Zhu, Z., Zhao, S., Li, X., Qu, K., & Lin, T.: Filter-free photonic frequency sextupler
732 operated over a wide range of modulation index. Optics & Laser Technology, 90, 144-148
733 (2017)

Figures

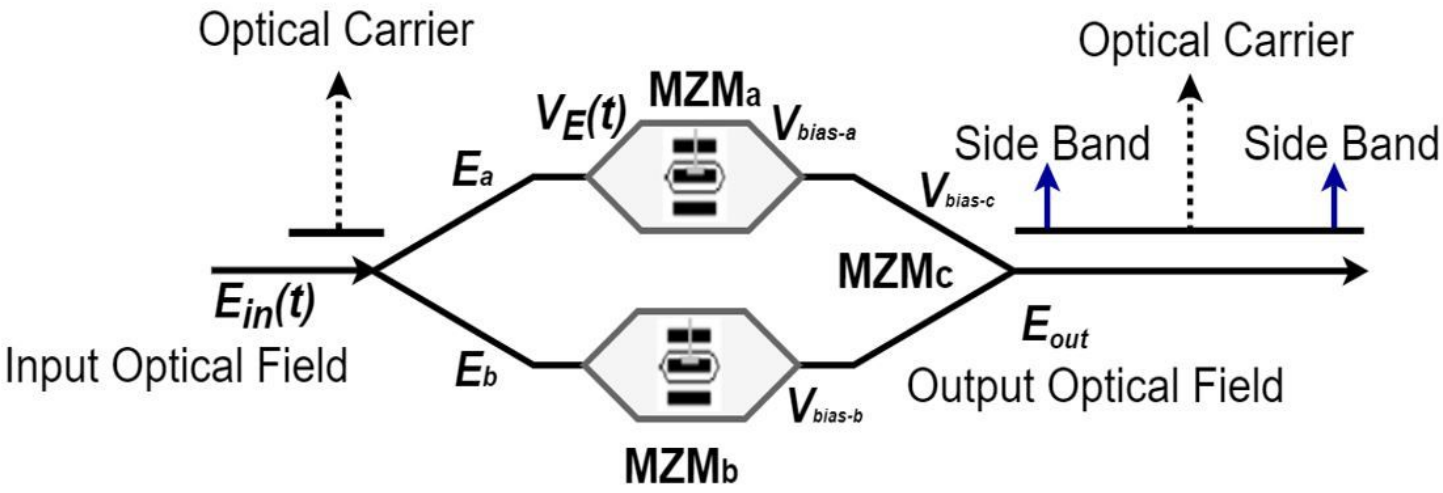

Figure 1

Conceptual diagram of a Dual Parallel Mach-Zehnder Modulator (DP-MZM).

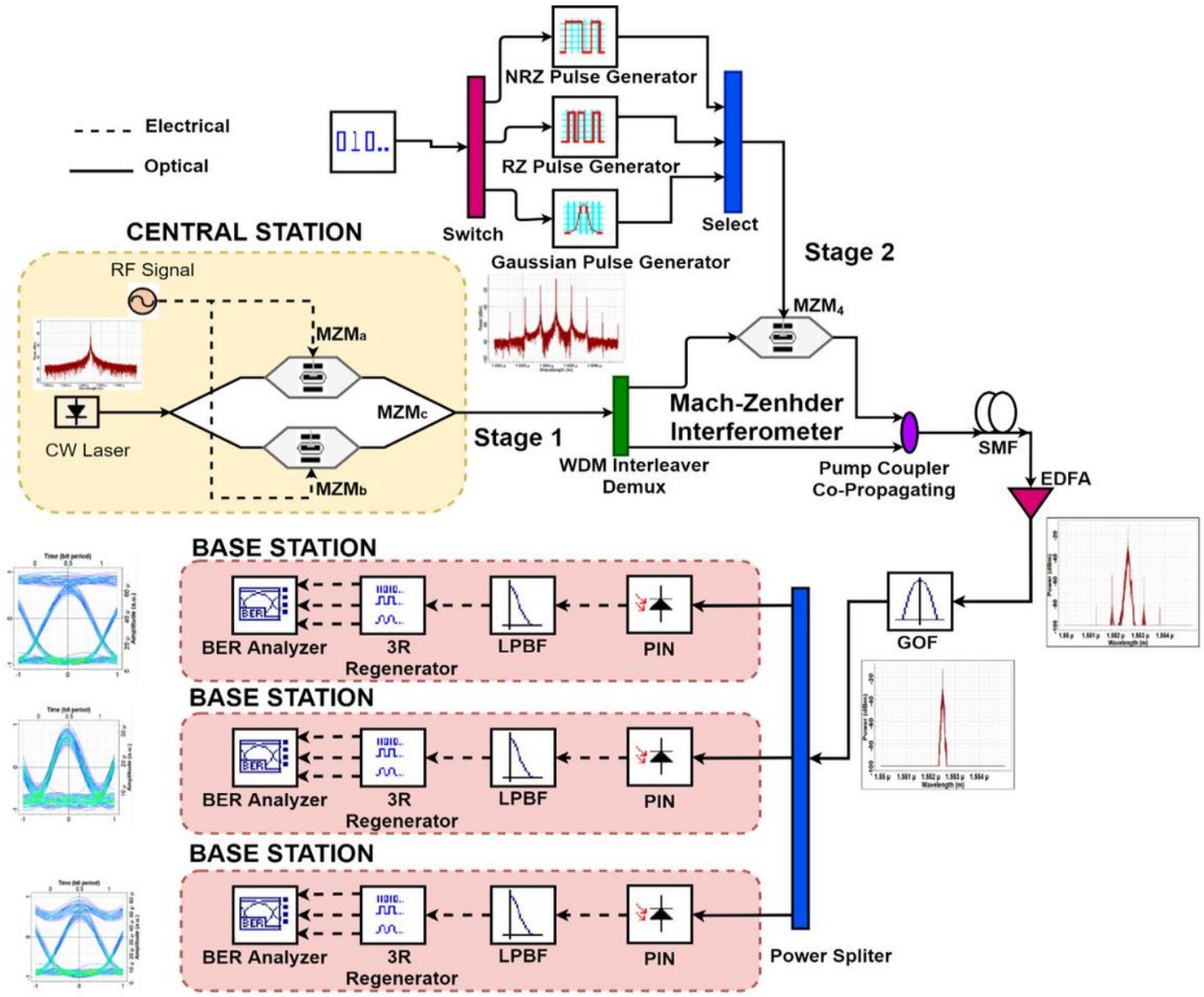

Figure 2

Schematic of the RoF-DP-MZM system proposed with three coding formats (NRZ, RZ and Gaussian).

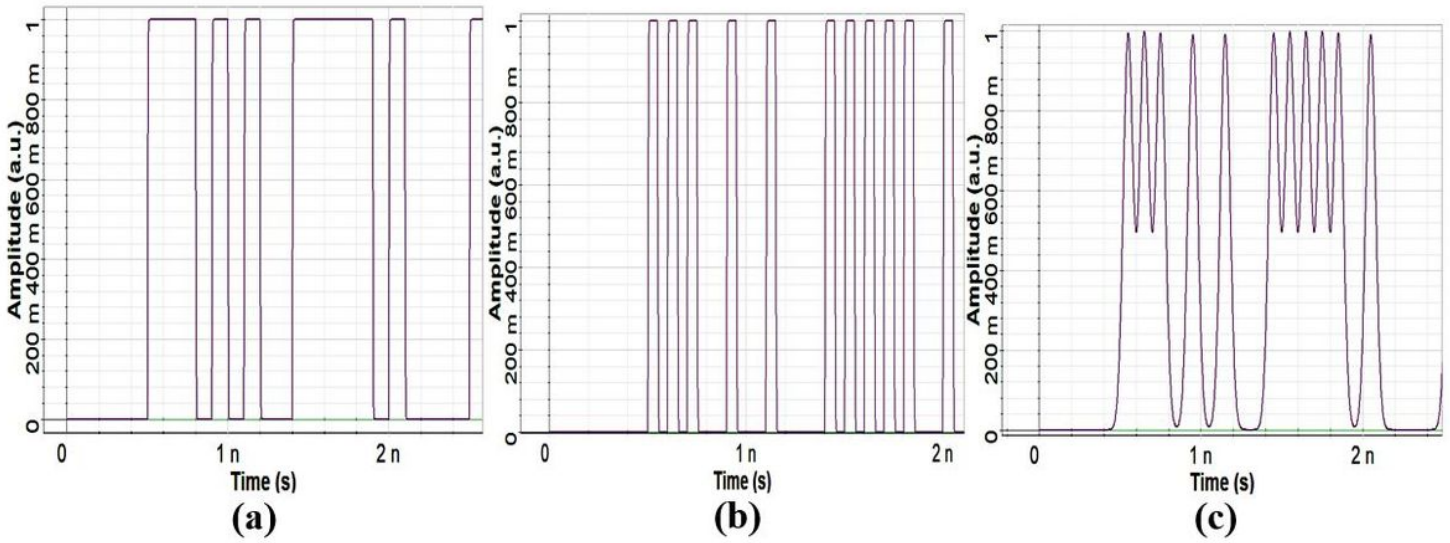

Figure 3

(a) NRZ pulse, (b) RZ pulse and (c) Gaussian Pulse.

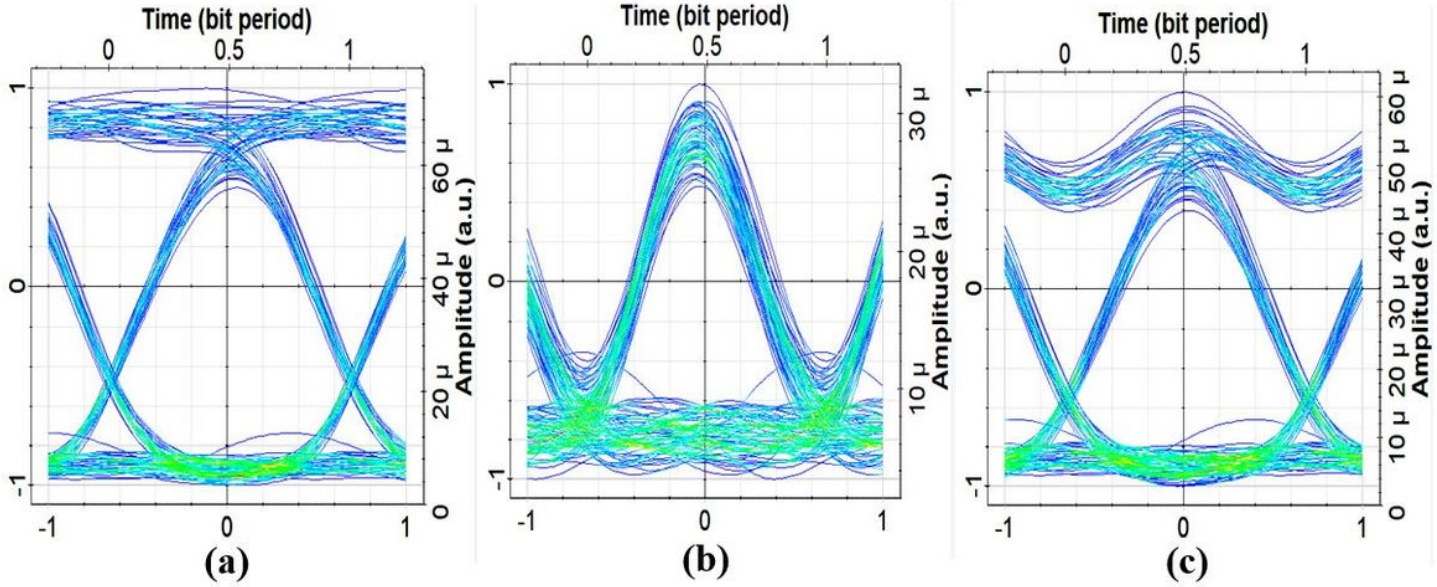

Figure 4

Eye diagram of the received signal for 20GHz mm-wave and for pulse formats NRZ (a), RZ (b) and Gaussian (c).

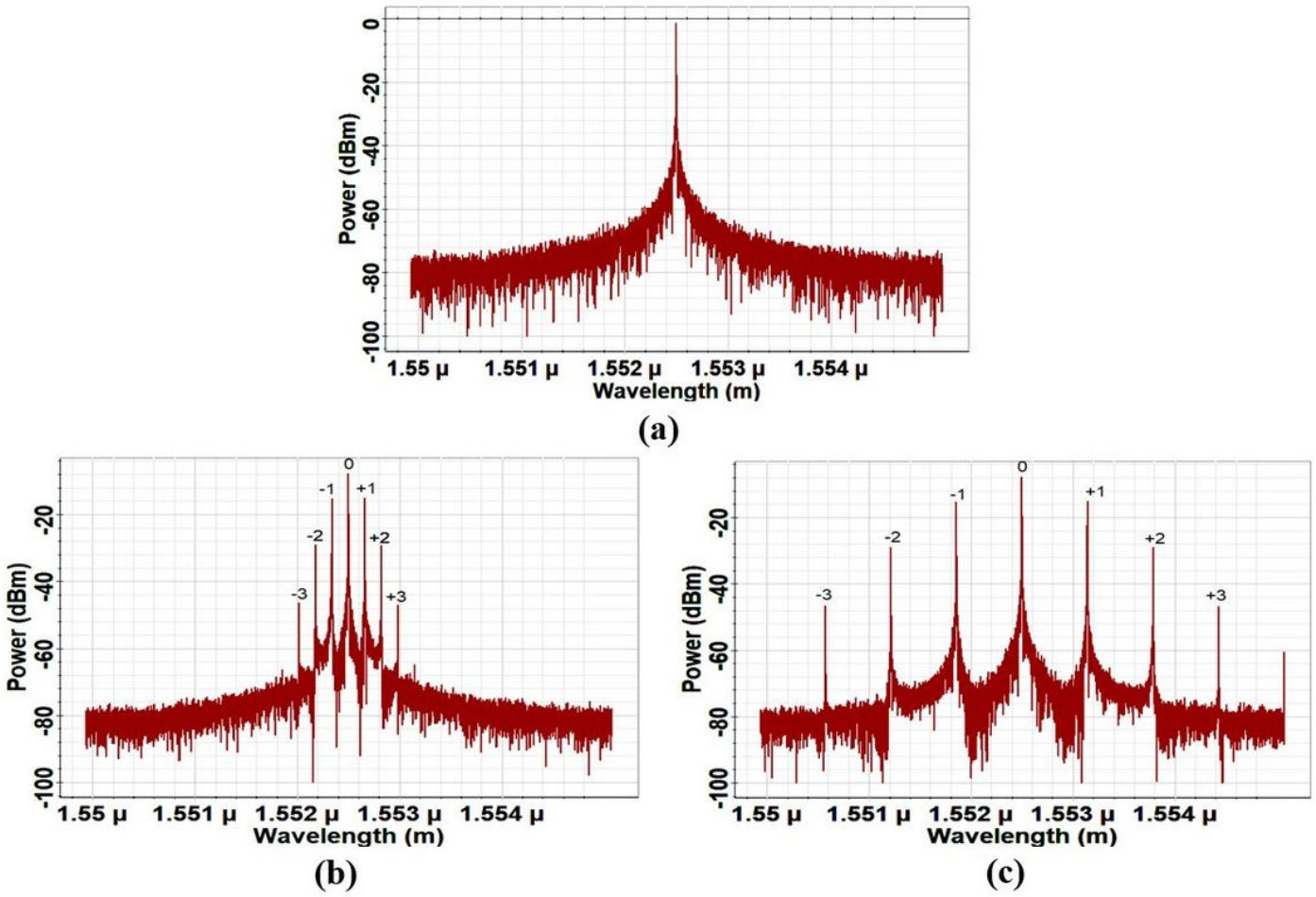

Figure 5

Transmitted signal at BS: Output Spectrum of the CW Laser (carrier) (a) and Spectra periodic optical sidebands at the DP-MZM output for the mm-wave frequency equal to 20 GHz (b) and 80 GHz (c), respectively.

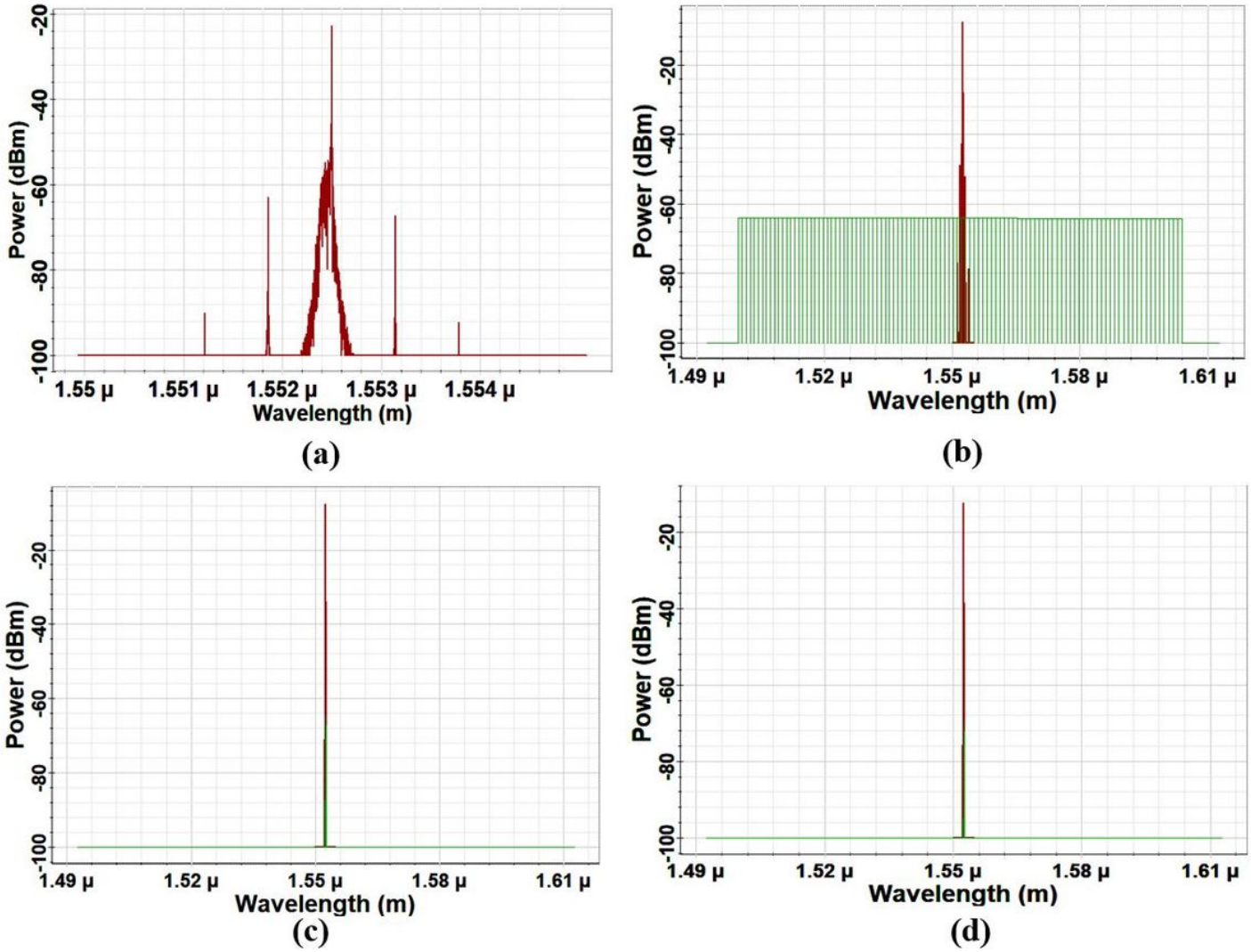

Figure 6

Optical Signal Spectrum at the WDM interleaver Demux (a), EDFA (b) GOF (c) and of BSs (d) outputs.

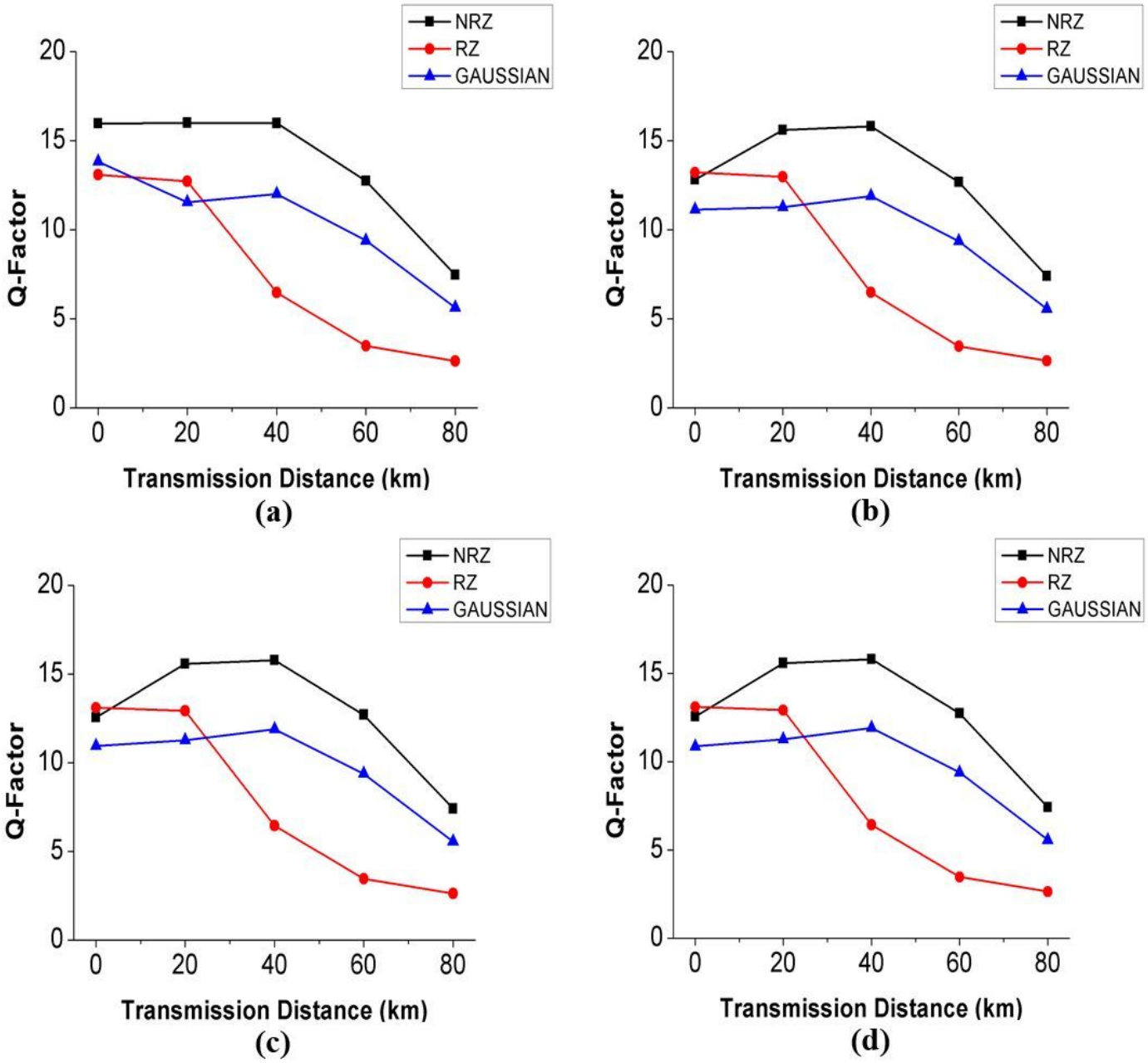

Figure 7

Q-Factor versus transmission distance for Downstream data of 20GHz (a), 40GHz (b), 60GHz (c) and 80GHz (d) for baseband signals with NRZ, RZ and Gaussian encoding.

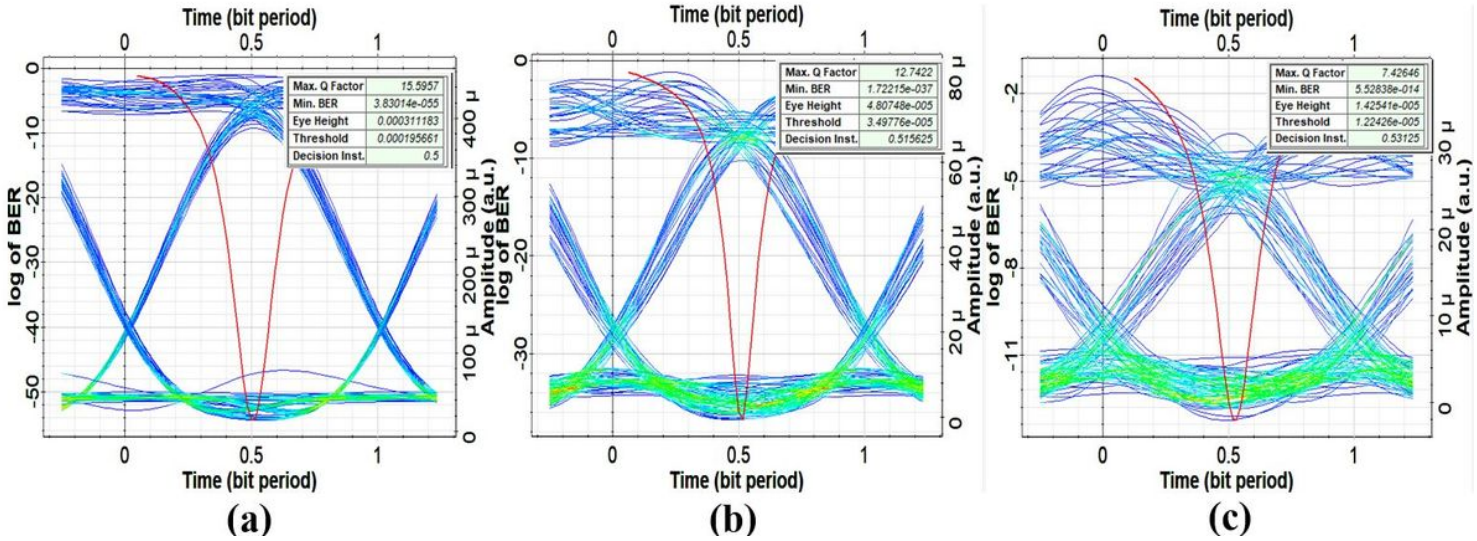

Figure 8

Eye diagram for the proposed RoF system with (a) 20km and (b) 60km and (c) 80km, both for 80GHz downstream data of NRZ encoding.

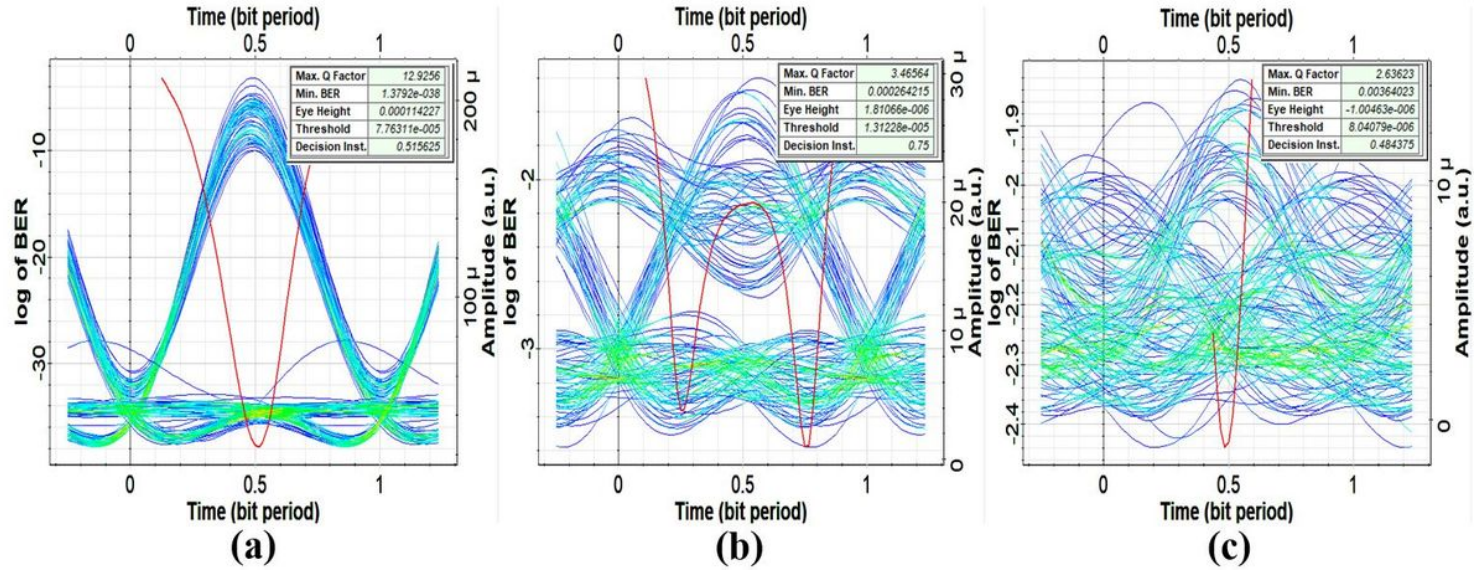

Figure 9

Eye diagram for the proposed RoF system with (a) 20km, (b) 60km and (c) 80km, both for RZ encoding 80GHz downstream data.

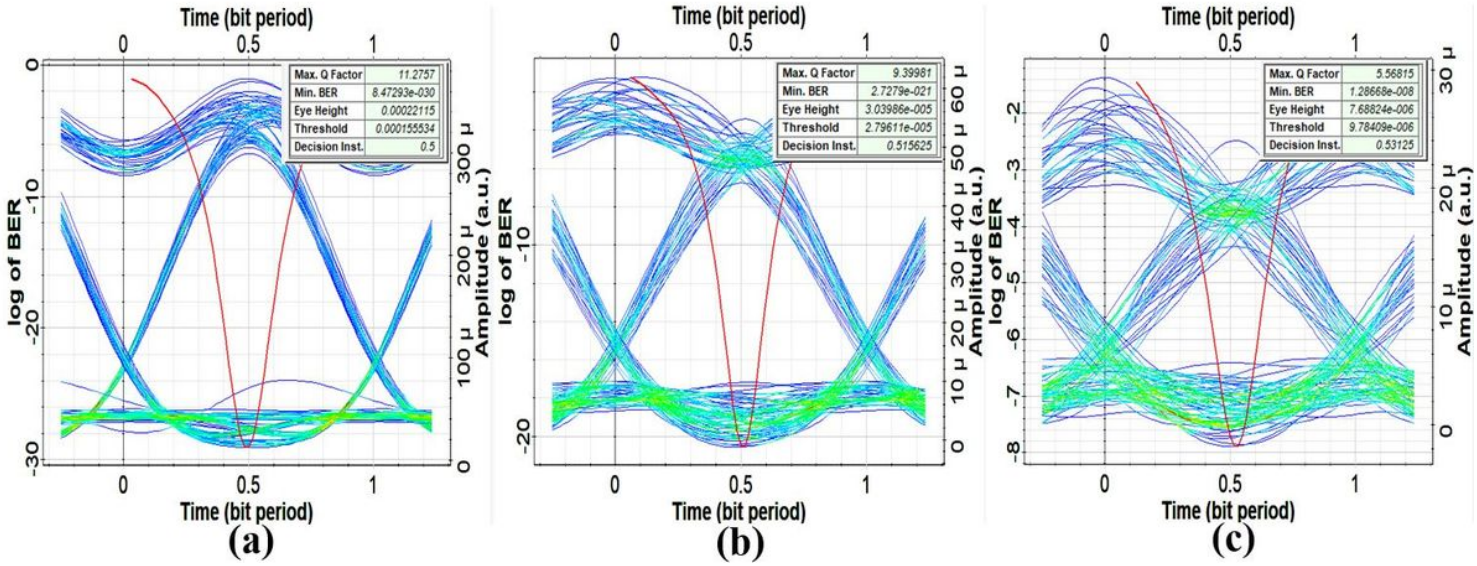

Figure 10

Eye diagram for the proposed RoF system with (a) 20km, (b) 60 km and (b) 80km, both for 80GHz downstream gaussian encoding data.

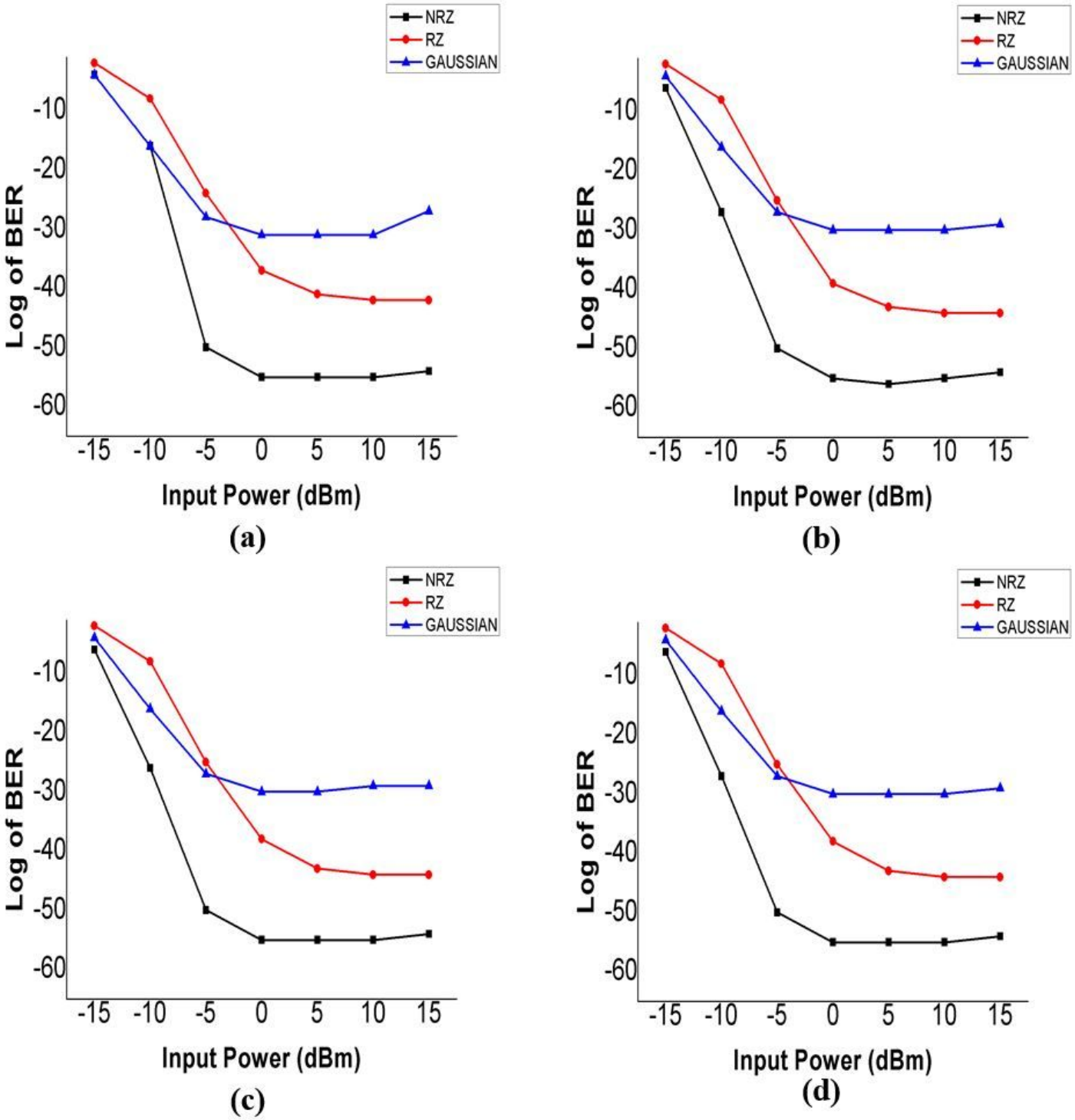

Figure 11

Log BER versus Input Power for Downstream data of 20GHz (a), 40GHz (b), 60GHz (c) and 80GHz (d) for baseband signals with NRZ, RZ and Gaussian coding.

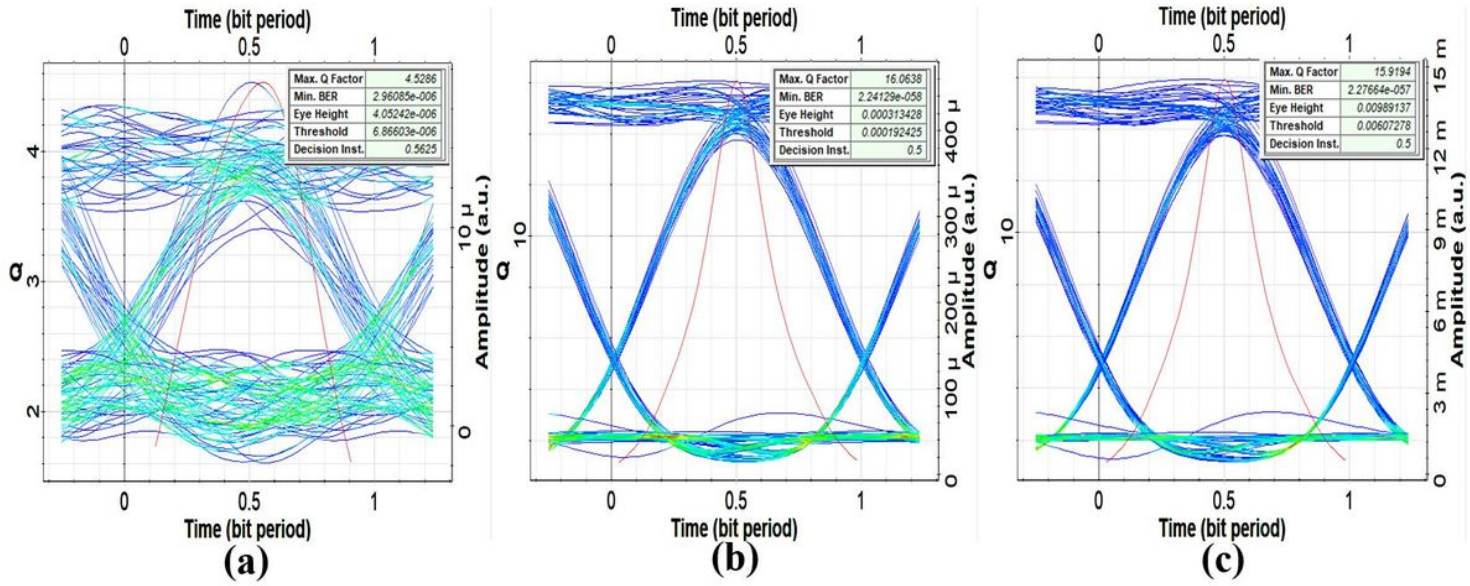

Figure 12

Eye diagram at, (a) -15dBm input power, (b) 0dBm input power and (c) 15dBm input power for the Non-Return-to-Zero (NRZ) coding signals.

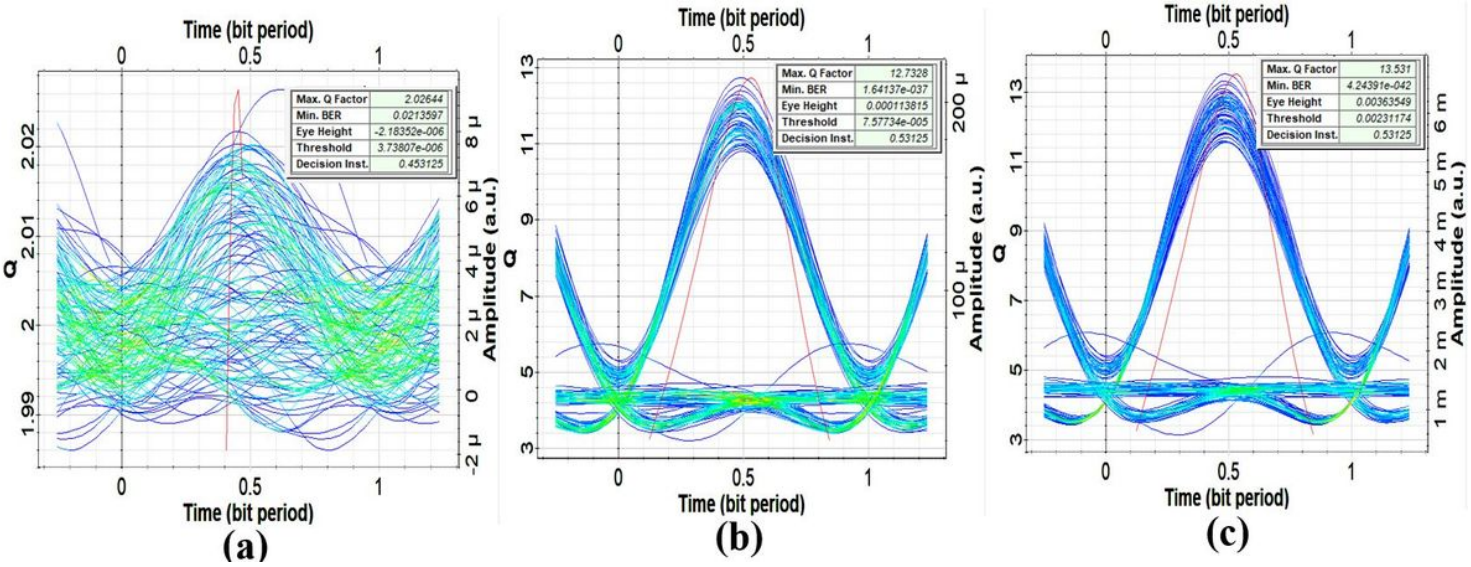

Figure 13

Eye diagram at, (a) -15dBm input power, (b) 0dBm input power and (c) 15dBm input power for the Return-to-Zero (RZ) coding signals.

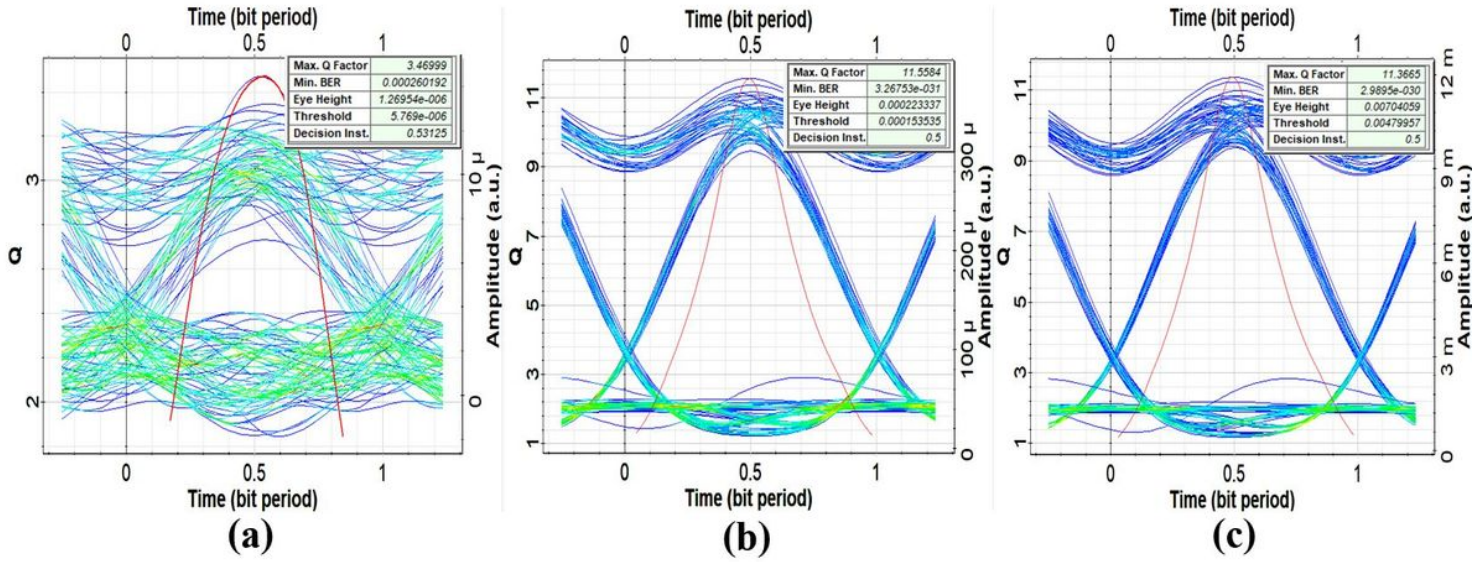

Figure 14

Eye diagram at, (a) -15dBm input power, (b) 0dBm input power and (c) 15dBm input power for the Gaussian encoding signals.